

ECOLOGY LETTERS

The three-species problem: incorporating competitive asymmetry and intransitivity in modern coexistence theory

Journal:	<i>Ecology Letters</i>
Manuscript ID	ELE-01043-2023.R1
Manuscript Type:	Letter
Date Submitted by the Author:	n/a
Complete List of Authors:	Ranjan, Ravi; Michigan State University, W.K. Kellogg Biological Station; Program in Ecology, Evolution and Behavior; Department of Plant Biology; Carl von Ossietzky University of Oldenburg, Helmholtz Institute of Functional Marine Biodiversity; Hanse-Wissenschaftskolleg Institute for Advanced Study Koffel, Thomas; Michigan State University, W.K. Kellogg Biological Station; Program in Ecology, Evolution and Behavior; Universite Claude Bernard Lyon 1, Laboratoire de Biométrie et Biologie Evolutive UMR5558 Klausmeier, Christopher; Michigan State University, W. K. Kellogg Biological Station; Program in Ecology, Evolution and Behavior; Department of Plant Biology; Department of Integrative Biology; Carnegie Institution for Science, Department of Global Ecology

SCHOLARONE™
Manuscripts

1
2
3 1 The three-species problem: incorporating competitive asymmetry and
4 2 intransitivity in modern coexistence theory
5
6

7 3 Ravi Ranjan^{1,2,3,4,5}, Thomas Koffel^{1,2,6}, Christopher A. Klausmeier^{1,2,3,7,8}
8
9

10 4 ¹ W.K. Kellogg Biological Station, Michigan State University, Hickory Corners, Michigan 49060
11 5 USA
12
13

14 6 ² Program in Ecology, Evolution and Behavior, Michigan State University, East Lansing, Michigan
15 7 48824 USA
16
17

18 8 ³ Department of Plant Biology, Michigan State University, East Lansing, Michigan 48824 USA
19
20

21 9 ⁴ Present address: Helmholtz Institute of Functional Marine Biodiversity (HIFMB), University of
22 10 Oldenburg, Ammerländer Heerstraße 231, D-26129 Oldenburg, Germany
23
24

25 11 ⁵ Hanse-Wissenschaftskolleg Institute for Advanced Study, Delmenhorst, Germany
26
27

28 12 ⁶ Present address: Université de Lyon, Université Lyon 1, CNRS, Laboratoire de Biométrie et
29 13 Biologie Evolutive UMR5558, Villeurbanne, France
30
31

32 14 ⁷ Department of Integrative Biology, Michigan State University, East Lansing MI 48824 USA
33
34

35 15 ⁸ Department of Global Ecology, Carnegie Institution for Science, Stanford CA 94305 USA
36
37

38 16 **Corresponding author email:** klausme1@msu.edu (Christopher A. Klausmeier)
39
40

41 17 **Short running title:** Three-species competition
42
43

44 18 **Keywords:** multispecies coexistence, competition, intransitive competition, modern
45 19 coexistence theory, structural stability, communities, Lotka-Volterra competition
46
47

48 20 **Manuscript type:** Letter
49
50

51 21 Number of words in the abstract: 148
52
53

54 22 Number of words in the main text: 4987
55
56

57 23 Number of words in each text box: 0
58
59
60

1
2
3 24 **Number of references:** 34
4
5 25 **Number of figures, tables and text boxes:** 6, 0 and 0
6
7 26 **Statement of authorship:** RR, TK and CAK jointly developed the theory. RR performed initial
8 analyses using code written by CAK and RR, and TK and CAK contributed substantially to further
9 analyses. RR wrote the first draft of the manuscript, which TK and CAK revised. CAK obtained
10 funding and supervised.
11
12
13
14
15
16
17
18 30 **Data Availability Statement:** The study uses no data. The code is available for review at
19
20 31 <https://github.com/cklausme/lv3> and will be permanently archived upon publication.
21
22
23
24
25
26
27
28
29
30
31
32
33
34
35
36
37
38
39
40
41
42
43
44
45
46
47
48
49
50
51
52
53
54
55
56
57
58
59
60

For Review Only

32 Abstract

33 While natural communities can contain hundreds of species, modern coexistence theory
34 focuses primarily on species pairs. Alternatively, the structural stability approach considers the
35 feasibility of equilibria, gaining scalability to larger communities but sacrificing information
36 about dynamic stability. Three-species competitive communities are a bridge to more-diverse
37 communities. They display novel phenomena while remaining amenable to mathematical
38 analysis, but remain incompletely understood. Here, we combine these approaches to identify
39 the key quantities that determine the outcome of competition. We show that pairwise niche
40 overlap and fitness differences are insufficient to completely characterize competitive
41 outcomes, which requires a strictly triplet-wise quantity: cyclic asymmetry. Low pairwise niche
42 overlap stabilizes the triplet, while high fitness differences promote competitive exclusion. The
43 effect of cyclic asymmetry on stability is complex and depends on pairwise niche overlap. In
44 summary, we elucidate how pairwise niche overlap, fitness differences, and cyclic asymmetry
45 determine the outcome of three-species competition.

38 46 1. Introduction

41 47 Modern coexistence theory (MCT) is a widely used theoretical framework for
42 48 understanding species coexistence. MCT has two broad strands (Song et al. 2019), with roots in
43 49 either the Lotka-Volterra competition model (Chesson, 1990) or invasion analysis (Barabás et
44 50 al., 2018; Chesson, 2000, 2018). Both strands define two quantities that determine the
45 51 outcome of competition: niche overlap and fitness differences. Niche overlap is thought to
46 52 measure resource use overlap and fitness differences to measure differences in innate

1
2
3 53 competitive ability. Lower niche overlaps generally lead to a more stable community while
4
5 54 higher fitness differences promote competitive exclusion.
6
7
8

9 55 Despite its success, MCT has focused primarily on pairwise competition. Extension to
10
11 56 multispecies competition has proven challenging, which first becomes apparent when moving
12
13 57 from two to three species. In multispecies competition, the term ‘fitness difference’ is a
14
15 58 misnomer: unlike usual difference operations, the fitness differences within two pairs of species
16
17 59 ($A \& B; B \& C$) does not determine the fitness difference between A and C . Therefore, fitness
18
19 60 differences as defined in MCT are relative, meaningful only in the context of specific pairs of
20
21 61 species, which impairs their application to more-diverse communities. This issue also holds for
22
23 62 niche differences, which also do not extend beyond pairs. Further, the invasion analysis strand
24
25 63 of MCT is based on mutual invasibility (Barabás et al., 2018; Chesson, 2000, 2018). In a
26
27 64 community of N species, mutual invasibility requires a positive invasion rate of each species
28
29 65 when rare into the long-term attractor of the community of $N - 1$ remaining species
30
31 66 (Armstrong & McGehee, 1976; Hofbauer & Schreiber, 2022). However, this requires that all of
32
33 67 the resident communities with $N - 1$ species persist without the invader present. While this is
34
35 68 easy to achieve in species pairs, where resident communities are simple monocultures, more
36
37 69 sub-communities are likely to be infeasible in diverse communities. Thus, the application of
38
39 70 invasion-based techniques to more-diverse communities is challenging (Barabás et al., 2018;
40
41 71 Hofbauer & Schreiber, 2022).

42
43
44
45
46
47
48
49
50
51 72 Three-species competition represents a significant jump in complexity, both in number
52
53 73 of parameters and dynamical phenomena. The addition of just one more species to the
54
55
56
57
58
59
60

1
2
3 74 pairwise Lotka-Volterra competition model increases the number of parameters from six to
4
5 75 twelve. In a triplet, intransitive competition can occur where each species can exclude one
6
7 76 species but is excluded by the other (rock-paper-scissors), leading to either stable coexistence
8
9 77 or a stable heteroclinic cycle (a trajectory that connects the boundary equilibria, approached as
10
11 78 ever-slowing oscillations) (Gilpin, 1975; May & Leonard, 1975). Since no pair of species can
12
13 79 coexist in isolation in intransitive competition, invasions are cyclic in nature and traditional
14
15 80 invasion analysis cannot determine the outcome of competition (Hofbauer, 1994; Hofbauer &
16
17 81 Schreiber, 2022). Besides heteroclinic cycles, three-species competition can result in other
18
19 82 novel phenomena such as limit cycles (Hofbauer & So, 1994) and various flavors of multiple
20
21 83 stable states. Figure 1 summarizes twenty-three distinct outcomes of three-species LV
22
23 84 competition. Three-species communities are the simplest that can exhibit indirect effects, yet
24
25 85 remain amenable to mathematical analysis, so we focus on them as a stepping stone to
26
27 86 understanding more complex communities and to illustrate the challenges of scaling up
28
29 87 pairwise approaches.

30
31
32
33
34
35
36
37
38 88 An alternative approach to multispecies communities focuses on the *structural stability*
39
40 89 of equilibria (Cenci & Saavedra, 2018; Saavedra et al., 2017). Structural stability considers the
41
42 90 feasibility of the equilibria (all species have positive abundance) — a necessary condition for
43
44 91 coexistence — and how this depends on environmental parameters. Calculating the feasibility
45
46 92 of equilibria is easy in Lotka-Volterra systems where it requires only inverting the community
47
48 93 matrix, allowing this approach to scale readily to larger communities. However, it ignores the
49
50 94 dynamic stability of a community, which is of ecological relevance: if a feasible community is
51
52 95 dynamically unstable, it is unlikely to be seen in nature. Further, the dynamical stability of a

1
2
3 96 community may even change within the structurally stable range of parameters. Therefore, the
4
5 97 structural stability approach may overstate the range of environments where species coexist.
6
7
8

9 98 Due to the limitations of both invasion-based and structural stability frameworks, a full
10
11 99 understanding of how multispecies communities persist remains elusive. In this study, we fill
12
13 100 this gap by combining perspectives of MCT, structural stability, and dynamical systems theory
14
15 101 to more-fully characterize three-species competition. We first partition pairwise fitness
16
17 102 differences in MCT into two quantities: absolute fitness differences and competitive
18
19 103 asymmetry. Next, we identify cyclic competitive asymmetry as the basis of intransitivity, a novel
20
21 104 outcome possible in triplets but not in pairs. We then systematically explore how cyclic
22
23 105 asymmetry, pairwise niche overlap and fitness differences combine to determine the outcome
24
25 106 of three-species competition. We start with symmetrical interactions but later remove this
26
27 107 assumption to show the generality of our results. We conclude by showing that in most cases,
28
29 108 the three-species competition outcome can be predicted using only six parameters, massively
30
31 109 reducing the dimensionality of the problem. All-in-all, this work develops a nearly complete
32
33 110 map of three-species competition outcomes as a function of cyclic asymmetry, niche overlaps
34
35 111 and fitness differences.

43
44 112

2. Model and Analysis

45
46 113 We study the \mathcal{N} -species Lotka-Volterra (LV) competition model ($\mathcal{N} = 2$ or 3)

47
48
49 115
$$\frac{dN_i}{dt} = \left(r_i - \sum_{j=1}^{\mathcal{N}} \alpha_{ij} N_j \right) N_i \quad (1)$$

50
51 116 where N_i is the density of species i . The intrinsic growth rate of species i is its growth rate
52
53
54
55
56
57
58
59
60

1
2
3 116 when alone at low density, denoted by r_i . We assume $r_i > 0$ so that each species can persist in
4
5 117 the absence of competition. The competition coefficients α_{ij} measure the per-capita
6
7 118 competitive impact of species j on species i , which is then summed across all species.
8
9

10
11 119 [2.1. Two-species competition](#)

12
13 120 We start with a brief summary of two-species LV competition (Chesson, 2020). The
14
15 121 invasion rate $\lambda_{i,j}$ of species i into the monoculture equilibrium of species j and vice versa ($\lambda_{j,i}$)
16
17
18 122 are:
19
20
21 123
$$\lambda_{i,j} = r_i - \frac{r_j \alpha_{ij}}{\alpha_{jj}}$$
 (2)
22
23
24 130
$$\lambda_{j,i} = r_j - \frac{r_i \alpha_{ji}}{\alpha_{ii}}$$
 (3)
25
26
27
28 124 For pairwise coexistence of i and j , both invasion rates must be positive ($\lambda_{i,j} > 0$ and $\lambda_{j,i} > 0$),
29
30
31 125 which results in the coexistence conditions
32
33
34 126
$$\sqrt{\frac{\alpha_{ii}\alpha_{jj}}{\alpha_{ij}\alpha_{ji}}} > \frac{r_i}{r_j} \sqrt{\frac{\alpha_{jj}\alpha_{ji}}{\alpha_{ii}\alpha_{ij}}} > \sqrt{\frac{\alpha_{ij}\alpha_{ji}}{\alpha_{ii}\alpha_{jj}}}$$
 (4)
35
36
37 127 MCT defines the niche overlap between species i and j as $\rho_{ij} = \sqrt{\frac{\alpha_{ij}\alpha_{ji}}{\alpha_{ii}\alpha_{jj}}}$, and their relative
38
39
40 128 fitness difference (technically, their fitness ratio) as $F_{ij} = \frac{r_i}{r_j} \sqrt{\frac{\alpha_{jj}\alpha_{ji}}{\alpha_{ii}\alpha_{ij}}}$. Therefore, species i and j
41
42
43
44 129 coexist if $0 \leq \rho_{ij} < 1$ and
45
46
47
48 131
$$\frac{1}{\rho_{ij}} > F_{ij} > \rho_{ij}$$
 (5)
49
50
51
52 132 Conversely, there is founder control ($\lambda_{ij} < 0$ and $\lambda_{ji} < 0$), also called *priority effects*, if $\rho_{ij} > 1$
53
54
55 133 (hyper niche-overlap) and
56
57
58
59
60

1
2
3 134 $\rho_{ij} > F_{ij} > \frac{1}{\rho_{ij}}$ (6)
4
5

6 135 (Chesson, 2020; Ke & Letten, 2018).
7
8
9

10 136 Expanding on MCT, we decompose the fitness difference between species i and j , F_{ij} ,
11
12 137 into the product of the ratio of intrinsic growth rates $R_{ij} = r_i/r_j$ and a combination of the
13
14 138 competition coefficients that measures *competitive asymmetry* A_{ij} :
15
16
17

18 139 $F_{ij} = R_{ij}A_{ij}$, where $A_{ij} = \sqrt{\frac{\alpha_{jj}\alpha_{ji}}{\alpha_{ii}\alpha_{ij}}}$ (7)
19
20
21

22 140 Because each species' intrinsic growth rate depends only on its fit to the abiotic environment,
23
24 141 we call R_{ij} the *absolute* fitness difference between species i and j . For fixed r_i values,
25
26 142 competitive asymmetry can change the outcome of competition, but across the range of fitness
27
28 143 differences it has only a quantitative effect, recentering the range of fitness differences that
29
30 144 result in coexistence or founder control at $R_{ij} = 1/A_{ij}$. However, it will prove key in
31
32 145 understanding three-species competition below.
33
34
35
36
37

38 146 2.2. Three-species competition: the dimensionality of parameter-space
39
40

41 147 How much more complex is three-species competition compared to two-species? The
42
43 148 two-species LV model has six parameters — two intrinsic growth rates and four competition
44
45 149 coefficients — which can be reduced to three through nondimensionalization (Appendix D), two
46
47 150 of which can be effectively combined by recentering. This leaves a two-dimensional space of
48
49 151 outcomes, which can be parameterized by either the invasion growth rates $\lambda_{i,j}$ and $\lambda_{j,i}$ or by
50
51 152 niche overlap ρ_{ij} and fitness difference $F_{ij} = R_{ij}A_{ij}$ (eqns. 5–7). A large competitive
52
53
54
55
56
57
58
59
60

1
2
3 153 asymmetry within a pair can be offset by an inverse absolute fitness difference, leading to a
4
5 154 fitness difference close to 1, which is at the center of the pairwise coexistence region.
6
7
8

9 155 Adding a third competitor illustrates a subtlety in the definition of fitness differences in
10
11 156 MCT. One might suppose that the fitness difference F_{ij} is the difference (technically, the ratio)
12
13 157 between the fitness of species i and j , that is, $F_{ij} = F_i/F_j$ for some appropriate definition of F_i .
14
15 158 If that were true, then knowing the fitness difference between species 1 and 2 (F_{12}) and that
16
17 159 between species 2 and 3 (F_{23}) would dictate the fitness difference between species 1 and 3 to
18
19 160 be $F_{13} = \frac{F_1}{F_3} = \frac{F_1}{F_2} \cdot \frac{F_2}{F_3} = F_{12}F_{23}$. Yet, the definition of fitness differences in eqn. 7 shows that is
20
21 161 not generally true, due to the competitive asymmetries A_{ij} . Therefore, fitness differences
22
23 162 between two species must be seen as relative to that particular pair of species and not
24
25 163 reflecting the difference between any species-specific fitnesses — an apparent contradiction.
26
27
28 164 On the other hand, the absolute fitness differences $R_{ij} = r_i/r_j$ are based on species-specific
29
30 165 fitnesses (r_i) and have the desirable property that $R_{13} = R_{12}R_{23}$. Thus, following Saavedra et al.
31
32
33 166 (2017), we will use the intrinsic growth rates r_i as a measure of a species' match to the abiotic
34
35 167 environment.

41
42
43 168 Following Eqns. 5–7, the outcomes of the three *pairwise* competitions among the three
44
45 169 species are determined by six invasion growth rates ($\lambda_{1,2}, \lambda_{2,1}, \lambda_{2,3}, \lambda_{3,2}, \lambda_{1,3}$, and $\lambda_{3,1}$) or
46
47 170 equivalently, by three niche overlaps (ρ_{12}, ρ_{23} and ρ_{31}) and three relative fitness differences
48
49 171 (F_{12}, F_{23} and F_{31}) — six parameters (note the cyclic ordering of subscripts). However, if we use
50
51 172 the absolute fitnesses r_i for the reasons described above, then we lose a degree of freedom
52
53 173 since $R_{12}R_{23}R_{31} = \frac{r_1}{r_2} \cdot \frac{r_2}{r_3} \cdot \frac{r_3}{r_1} = 1$, leaving only five independent parameters. What is the
54
55
56
57
58
59
60

1
2
3 174 missing parameter encoded in the three relative fitness differences F_{ij} that cannot be found in
4
5 175 the two independent r_i 's? Inspired by Klimenko (2015), we suggest the missing parameter is
6
7 176 the geometric mean of the competitive asymmetries A_{ij} ,
8
9

10
11
12 177
$$\bar{A} = \sqrt[3]{A_{12}A_{23}A_{31}} = \sqrt[6]{\frac{\alpha_{21}\alpha_{13}\alpha_{32}}{\alpha_{12}\alpha_{31}\alpha_{23}}} \quad (8)$$

13
14
15

16
17 178 which we term the *cyclic asymmetry* of the triplet.
18

19
20
21 179 The cyclic asymmetry \bar{A} measures the nonadditivity of competition among the three
22 species. When $\bar{A} = 1$, $F_{12}F_{23}F_{31} = 1$ and intransitivity is impossible. Deviation of \bar{A} from 1
23
24 180 signals that the triplet is potentially intransitive, and higher deviations signal higher potential
25
26 181 intransitivity. Intransitivity can go in one direction ($1 \rightarrow 2 \rightarrow 3 \rightarrow 1$) or the other ($1 \rightarrow 3 \rightarrow 2 \rightarrow$
27
28 182 1), reflected by $\bar{A} > 1$ or $\bar{A} < 1$, respectively. Thus, permuting species labels can flip the
29
30 183 relative position of \bar{A} with respect to 1, replacing \bar{A} with its reciprocal.
31
32 184

33
34
35
36 185 Moving beyond the pairwise competitive outcomes discussed above to consider the full
37
38 186 three-species competition, the total number of parameters of three-species Lotka-Volterra
39 competition is twelve — three intrinsic growth rates and nine competition coefficients. This can
40
41 187 be reduced to eight through nondimensionalization (Appendix D), but an exhaustive
42
43 188 exploration of parameter-space remains challenging. We will present our results in terms of
44
45 189 three intrinsic growth rates (r_1 , r_2 , and r_3), three pairwise niche overlaps (ρ_{12} , ρ_{23} , and ρ_{31}),
46
47 190 and three competitive asymmetries (A_{12} , A_{23} , and A_{31}). To facilitate comparison with the
48
49 191 structural stability framework (Saavedra et al., 2017), we assume without loss of generality $r_1 +$
50
51
52 192

1
2
3 193 $r_2 + r_3 = 1$, which reduces the total number of parameters to eight (3+3+3-1=8), consistent
4 with the nondimensionalization. We assume that the r_i 's represent species responses to the
5 underlying environment and that the competition coefficients / measures of niche overlap and
6 competitive asymmetry are constant for a set of species.
7
8
9
10
11
12
13

14 197 [2.3. Three-species competition: analysis](#)

15
16 198 Following Saavedra *et al.* (2017), we present our results in the unit simplex $r_1 + r_2 +$
17
18 199 $r_3 = 1$ to illustrate how species' intrinsic growth rates influence the outcomes of competition
20
21 200 (see Appendix B for details about how to interpret the simplex). Saavedra and colleagues
22
23 201 focused on the *structural stability* of an equilibrium, *i.e.*, the environmental range under which
24
25 202 the equilibrium is feasible. For simplicity, they assume that the matrices of competition
26
27 203 coefficients are either positive definite or Volterra-dissipative (Saavedra *et al.* 2017 Appendix
28
29 204 S1), which implies $\rho_{ij} < 1$ for all pairs and global stability of all coexisting communities and
30
31 205 subcommunities. Under this assumption, the feasibility of an equilibrium implies its global
32
33 206 stability. However, $\rho_{ij} > 1$ results in alternative stable states in pairs (Ke & Letten 2018).
34
35 207 Therefore, focusing solely on feasibility as in the structural stability framework may
36
37 208 overestimate the environmental conditions under which species coexist. Thus, a fuller
38
39 209 understanding of the outcome of three-species competition requires the consideration of
40
41 210 *dynamical* stability.
42
43
44
45
46
47
48
49
50
51
52
53
54
55
56
57
58
59
60

211 We numerically assess the feasibility and stability of all equilibria, consisting of the full
212 community (the unique three-species equilibrium) and all of its subcommunities (three one-
213 species and three two-species equilibria), using local stability analysis. In the case of

1
2
3 214 subcommunities, this can be simplified to invasion analysis, combining Eqns. 5–7 with the
4
5 215 invasion growth rate of missing species ($\lambda_{inv,res}$ for species inv invading resident community
6
7 216 res). We apply Routh-Hurwitz criteria to check the stability of the three-species equilibrium if it
8
9 217 is feasible. Finally, if a heteroclinic cycle exists from species $i \rightarrow j \rightarrow k \rightarrow i$ ($\lambda_{j,i} > 0 > \lambda_{i,j}$,
10
11 218 $\lambda_{k,j} > 0 > \lambda_{j,k}$, and $\lambda_{i,k} > 0 > \lambda_{k,i}$), we check its stability using the Hofbauer criterion
12
13 219 (Hofbauer & Sigmund, 1998). See Appendix A for details of our mathematical analysis.
14
15
16
17
18
19 220 We summarize the outcome of competition across the $r_1 - r_2 - r_3$ simplex. There are at
20
21 221 least twenty-three qualitatively different outcomes possible, with a large number of alternative
22
23 222 stable states (Zeeman 1993). To visually communicate this, we use a color scheme based on the
24
25 223 traditional red-yellow-blue color model (Fig. 1). Monocultures are shown as primary colors.
26
27
28 224 Stable coexistence of a pair is shown as secondary colors formed by mixing the corresponding
29
30 225 monocultures' primary colors. Alternative stable states are shown with stripes whose colors
31
32 226 correspond to the alternative outcomes. Stable equilibrium three-species coexistence is
33
34 227 denoted by gray, stable heteroclinic cycles are denoted by spirals and limit cycles are denoted
35
36 228 by white.

42 229 2.4 Three-species competition: results

43
44 230 Due to the eight-dimensional parameter space, we present various special cases that
45
46 231 embed various symmetries in the parameters. We begin by varying the number of stably
47
48 232 coexisting pairs ($\rho_{ij} < 1$) versus those with founder control ($\rho_{ij} > 1$). We then examine the
49
50 233 role of cyclic asymmetry by considering equal asymmetry between species ($A_{12} = A_{23} = A_{31} =$
51
52 234 $\bar{A} > 1$). We then investigate the combined role of niche overlap ($\rho_{12} = \rho_{23} = \rho_{31} = \rho$) and

1
2
3 235 cyclic asymmetry (\bar{A}). Finally, we present more cases that break these symmetries, and provide
4
5 236 code as a supplement for readers to explore further.
6
7
8

9 237 *Pairwise coexistence vs. founder control.* Depending on the pairwise niche overlap
10
11 238 among species, structural and dynamical stability can have a complex relationship (Fig. 2). The
12
13 239 left column of Fig. 2 (Figs. 2aceg) shows the feasibility regions of the three-species equilibrium
14
15 240 (dark gray triangle) and of the three pairwise equilibria, with color indicating their pairwise
16
17 241 stability (coexistence in orange and founder control in lavender). See Appendix B for a detailed
18
19 242 explanation about the construction and interpretation of these plots. The right column shows
20
21 243 the outcome of competition. Note that we chose an especially symmetrical case for
22
23 244 demonstration, where all the feasibility regions are centered on the centroid of the simplex
24
25 245 ($r_1 = r_2 = r_3 = 1/3$); we will see below that this case has no cyclic asymmetry ($\bar{A} = 1$). There
26
27 246 are four different combinations of stability between the pairs: 0 (Fig. 2ab), 1 (Fig. 2cd), 2 (Fig.
28
29 247 2ef) and all 3 (Fig. 2gh) pairs with founder control.
30
31
32
33
34
35
36

37 248 The distinction between feasibility of equilibria and competitive outcomes plots is
38
39 249 immediately apparent (Fig. 2) (see Appendix C for more details). Only in the first row (Fig. 2ab)
40
41 250 where all three pairs can potentially coexist, does three-species feasibility translate into three-
42
43 251 species coexistence (gray in both Fig. 2a and b). In cases with more pairwise founder control
44
45 252 (Figs. 2c-h), the relationship between feasibility and competitive outcomes becomes more
46
47 253 complex. Pairwise founder control impacts even the region where the three-species
48
49 254 equilibrium is feasible (gray region in the center, left column), where the competitive outcome
50
51 255 is a variety of alternative stable states (striped regions, right column), not three-species
52
53
54
55
56
57
58
59
60

1
2
3 256 coexistence. When all three species show founder control (Fig. 2gh), the competitive outcome
4
5 257 at the center of the $r_1 - r_2 - r_3$ simplex is a three-way founder control between the three
6
7 258 monocultures (red, yellow and blue stripes in the center). Surprisingly, this occurs over a much
8
9 259 larger region than the gray feasibility region of the three-species equilibrium in the feasibility
10
11 260 plot. Therefore, the competitive outcome in this case is not directly related to the feasibility of
12
13 261 the three-species equilibrium.

17
18
19 262 *Cyclic asymmetry & intransitivity.* In pairwise competition, competitive asymmetry A_{ij}
20
21 263 only recenters the range of absolute fitness differences R_{ij} that lead to coexistence or founder
22
23 264 control (eqn. 8). However, in three-species communities, this recentering is not completely
24
25 265 possible when $\bar{A} \neq 1$.

28
29
30 266 When there is no cyclic asymmetry ($\bar{A} = 1$, Fig. 2 and Fig. 3ab), the stabilizing pairwise
31
32 267 niche overlap plays the dominant role in determining competition outcome. Each pair can
33
34 268 coexist when the environment favors neither species in the pair. Similarly, the triplet can
35
36 269 coexist stably when the environment is relatively balanced between all three species. The lack
37
38 270 of cyclic asymmetry can be seen in Fig. 3a, where all three pairwise equilibria regions (orange
39
40 271 triangles) intersect at the same location, maximizing their overlap. Consequently, the three-
41
42 272 species equilibrium is both feasible (gray triangle, Fig. 3a) and stable (gray triangle, Fig. 3b) at
43
44 273 the center.

45
46
47
48
49
50 274 Intermediate cyclic asymmetry (Fig. 3cd) promotes the conditions for an intransitive
51
52 275 rock-papers-scissors cycle: a parameter region where the three species equilibrium is feasible
53
54 276 but none of the pairwise equilibria are (shown with a dashed border in Fig. 3c). However, cyclic

1
2
3 277 asymmetry interacts with the low pairwise niche overlap so that the competitive outcome in
4
5 278 this region remains stable three-species coexistence (gray region, Fig. 3d). Graphically, the
6
7 279 competitive asymmetry within each pair twists the orange feasibility regions away from the
8
9 280 centroid of the simplex, representing the indirect positive effect of species 1 on species 3 due
10
11 281 to inhibiting species 2.

12
13
14
15
16 282 At high cyclic asymmetry (Fig. 3ef), the orange pairwise feasibility regions twist even
17
18 283 further, expanding the region where intransitivity occurs (Fig. 3e). For some values of the
19
20 284 intrinsic growth rates, the three-species equilibrium loses stability, resulting in a stable
21
22 285 heteroclinic cycle, which is approached with ever-slowing oscillations (Fig. 4a). In natural
23
24 286 communities, these cycles would result in monocultures due to finite population sizes.
25
26
27 287 However, even at high cyclic asymmetry, the parameter regions with heteroclinic cycles are
28
29 288 surrounded by regions of stable three-species coexistence (gray region in Fig. 3f, Fig. 4c) due to
30
31 289 the stabilizing pairwise niche overlaps in all pairs. In a narrow range of parameters in between
32
33 290 stable equilibria and stable heteroclinic cycles, there is a limit cycle where the three species
34
35 291 oscillate with a fixed period (the narrow white region around the region with heteroclinic cycles
36
37
38 292 in Fig. 3f, Fig. 4b).

39
40
41
42
43
44 293 *Interaction of cyclic asymmetry and niche overlap.* In a triplet, higher cyclic asymmetry
45
46 294 increases the proportion of environments where heteroclinic cycles occur (Fig. 3). How is this
47
48 295 influenced by pairwise niche overlap and fitness imbalances? For a more complete picture of
49
50 296 how these three quantities interact, we plot a series of outcome plots simultaneously varying

1
2
3 297 pairwise niche overlap and cyclic asymmetry (Fig. 5). We omit cyclic asymmetry values lesser
4
5 298 than one, because the results are symmetric.
6
7
8

9 299 Read Fig. 5 beginning at the center of the bottom row. The case of no cyclic asymmetry
10
11 300 ($\bar{A} = 1$) and complete niche overlap ($\rho = 1$) represents competition for a single resource:
12
13 301 coexistence is impossible and the winner is the species with the highest r_i value (Tilman 1985).
14
15 302 Moving to the left represents decreasing niche overlap between species, which increases the
16
17 likelihood of pairwise coexistence (left half of the bottom row). This is also a stabilizing
18
19 influence on the triplet, where the stable three-species equilibrium is found in a region that
20
21 304 increases in size with decreasing niche overlap, making the coexistence of all three species
22
23 305 more likely. In contrast, increasing niche overlap between pairs destabilizes the triplet, resulting
24
25 306 in no three-species coexistence. Further, the likelihood of alternative stable states increases
26
27 307 due to the presence of founder control in the pairs, as can be seen in the increased area of the
28
29 308 striped regions as niche overlap increases towards the right in the bottom row (Fig. 5).
30
31
32

33 310 Next, return to $\rho = 1, \bar{A} = 1$ and now move up to see the role of cyclic asymmetry in
34
35 311 isolation in absence of niche overlap. As in Fig. 3, increased cyclic asymmetry results in the
36
37 312 development of a region of parameter space with heteroclinic cycles (spiral regions). Higher
38
39 313 cyclic asymmetry leads to larger proportions of the environment where the competitive
40
41 314 outcome is heteroclinic cycles. At extremely high cyclic asymmetry ($\bar{A} = 8$), competition results
42
43 315 in heteroclinic cycles in almost all environments.
44
45
46

47 316 Overall, as in pairwise competition, low niche overlap stabilizes the triplet while high
48
49 317 niche overlap destabilizes it by creating alternative stable states. Cyclic asymmetry can
50
51
52
53
54
55
56
57
58
59
60

1
2
3 318 destabilize the system in a different way, creating environments where heteroclinic cycles
4
5 319 occur. How do these two forms of destabilization interact? At low values of niche overlap and
6
7 320 high cyclic asymmetry, the stabilizing influence of low niche overlap counteracts the
8
9 321 destabilizing effect of cyclic asymmetry (towards the left in the top row of Fig. 5). Thus, the
10
11 322 parameter space resulting in heteroclinic cycles reduces in area and is replaced by a stable
12
13 323 three-species equilibrium. Hyper niche-overlap ($\rho > 1$) also reduces the likelihood of
14
15 324 heteroclinic cycles, albeit by replacing them with alternative stable states which are also
16
17 325 destabilizing (towards the right in the top row of Fig. 5). Fig. S1 shows the stability of the
18
19 326 symmetric $r_1 = r_2 = r_3 = 1/3$ equilibrium, as shown in Fig. 1 of May & Leonard (1975) in terms
20
21 327 of our parameters ρ and \bar{A} , which supports these conclusions.

27
28
29 328 For a more complete picture of the interaction of pairwise niche overlap and cyclic
30
31 329 asymmetry on the likelihood of three-species coexistence, we plotted the proportion of the $r_1 -$
32
33 330 $r_2 - r_3$ simplex that results in stable three-species coexistence (Fig. 6). The dependence of
34
35 331 three-species coexistence on cyclic asymmetry and pairwise niche overlap is surprisingly
36
37 332 complex. At low niche overlap ($\rho < 0.25$), increasing cyclic asymmetry decreases the likelihood
38
39 333 of three-species coexistence. At intermediate niche overlap ($0.25 < \rho < 0.75$), the likelihood
40
41 334 of three-species coexistence is maximized at intermediate cyclic asymmetry. At higher niche
42
43 335 overlap ($\rho > 0.75$), three-species coexistence is unlikely. In all cases, increasing cyclic
44
45 336 asymmetry increases the proportion of environments that result in heteroclinic cycles.

1
2
3 337 2.5 Relaxing assumptions of symmetry
4

5 338 Aside from Fig. 3, we have assumed that all three pairs within the triplet have the same
6
7 339 niche overlap ($\rho_{12} = \rho_{23} = \rho_{31} = \rho$) and equal competitive asymmetry ($A_{12} = A_{23} = A_{31} =$
8
9
10 340 \bar{A}). Thus Fig. 5 represents only a four-dimensional slice through the full eight-dimensional
11
12 parameter space of the three-species LV competition model. We now relax these assumptions
13
14 341 in two ways.
15
16

17
18 343 *Numerical exploration.* To illustrate some of the further possible outcomes of three-
19 species competition, we break the symmetry of the ρ_{ij} 's by allowing one pair (1 and 3) to have
20
21 344 a different niche overlap than the other two. We choose the third pair's niche overlap to be the
22 reciprocal of the first two ($\rho_{12} = \rho_{23} = 1/\rho_{31}$), as to change the stability of the feasibility
23
24 345 regions while keeping their extent unchanged (as in Fig. 2). In Fig. S2, we reconstruct the
25
26 346 outcome plots while varying both different cyclic asymmetry and pairwise niche overlap. We
27
28 347 find more complex transitions along outcomes. We find the same general result as in Fig. 5, that
29
30 348 heteroclinic cycles occur with balanced intrinsic growth rates, large cyclic asymmetry, and
31
32 349 intermediate niche overlap. We also identified novel outcomes, such as alternative stable states
33
34 350 between one species and three-species coexistence (yellow-gray striped regions). Finally, we
35
36 351 see that three-species coexistence can be stable even when one pair of species experiences
37
38 352 founder control in isolation ($\rho > 1$) if there is also cyclic asymmetry (gray regions for $\bar{A} > 1$).
39
40
41

42
43 355 *Recentering.* Despite having three free parameters, the outcome of two-species LV
44 competition can be described by only two quantities (relative fitness difference F_{ij} and niche
45
46 356 overlap ρ_{ij}) by recentering absolute fitness difference $R_{ij} = r_i/r_j$ by the competitive
47
48 357 overlap ρ_{ij} by recentering absolute fitness difference $R_{ij} = r_i/r_j$ by the competitive
49
50
51
52
53
54
55
56
57
58
59
60

1
2
3 358 asymmetry A_{ij} (eqn. 7). Can the dimensionality of three-species LV competition be reduced
4
5 359 from its eight parameters in a similar way? The answer is a qualified “yes”: we can recover the
6
7 360 feasibility regions completely and most of the outcomes, but the stability of the three-species
8
9 361 equilibrium can change.
10
11

12
13
14 362 Our approach to recentering the growth rates is suggested by the pairwise coexistence
15
16 363 conditions
17
18

19
20 364
$$\frac{1}{\rho_{ij}} > A_{ij}R_{ij} > \rho_{ij} \quad (9)$$

21
22

23
24
25 365 To isolate the effect of cyclic asymmetry $\bar{A} = \sqrt[3]{A_{12}A_{23}A_{31}}$ from other aspects of competitive
26
27 366 asymmetry, we factor it out from the relative fitness difference $A_{ij}R_{ij}$:
28
29

30
31
32 367
$$\frac{1}{\rho_{ij}} > \bar{A} \frac{A_{ij}^{2/3}}{A_{ki}^{1/3}A_{jk}^{1/3}} R_{ij} > \rho_{ij}$$

33
34
35 368
$$\frac{1}{\rho_{ij}} > \bar{A} A'_{ij} R_{ij} > \rho_{ij} \quad (10)$$

36
37

38
39 368 Note that $A'_{12}A'_{23}A'_{31} = 1$, so that \bar{A} captures all of the cyclic asymmetry of the triplet. Breaking
40
41
42 369 up A'_{ij} as $A'_{ij} = \left(\frac{A_{ij}}{A_{ki}}\right)^{1/3} / \left(\frac{A_{jk}}{A_{ij}}\right)^{1/3}$, we see that by rescaling the r_i 's and using a different
43
44
45 370 constraint on them:
46
47

48
49 371
$$r_1 \left(\frac{A_{12}}{A_{31}}\right)^{1/3} + r_2 \left(\frac{A_{23}}{A_{12}}\right)^{1/3} + r_3 \left(\frac{A_{31}}{A_{23}}\right)^{1/3} = 1 \quad (11)$$

50
51

52
53 372 effectively recenters the feasibility plots (see also Saavedra et al. 2017 Appendix S5).
54
55
56
57
58
59
60

1
2
3 373 Figs. S3-4 illustrate the effect of this recentering procedure on feasibility regions and
4 outcome plots. In both cases, the feasibility regions are identical to those with equal $A_{ij} = \bar{A}$
5 after recentering (Figs. S3-4, compare c vs. e). The outcome plots are also largely the same after
6 recentering (Figs. S3-4, compare d vs. f), with the exception of the stability region of the three-
7 species coexistence equilibrium (gray vs. white regions in Fig. S4df). The case with unequal
8 asymmetries (Fig. S4d) presents a new outcome: alternative stable states between three-
9 species coexistence and a heteroclinic cycle, which we have verified numerically (Fig. S5ab),
10 along with limit cycles in the white region of Fig. S4d (Fig. S5c). Recentering effectively causes
11 the units of time in each species' equation to be different, therefore changing the parameter
12 ranges of time-dependent quantities such as limit cycles but not of static quantities such as
13 equilibria, which remain unaffected.

14
15
16 384 However, these residual effects of unequal asymmetries after recentering are largely
17 irrelevant to the question of species persistence: triplets that coexist at a stable equilibrium or
18 on a limit cycle still coexist, and a stable heteroclinic cycle still presents the risk of extinction in
19 a finite world. Therefore, recentering effectively preserves the outcome of competition,
20 although the dynamics may change. Thus, the outcome of three-species LV competition can be
21 largely captured using six parameters: three pairwise niche overlaps, two rescaled fitness ratios,
22 and cyclic asymmetry \bar{A} .

23 391 Discussion

24 392 Modern coexistence theory primarily relies on models of pairwise competition to
25 understand species coexistence. However, the extent to which insights from pairwise models

1
2
3 394 extend to more diverse communities remains unknown. In this study, we analyzed a three-
4 species competition model to demonstrate the limitations of applying insights from pairwise
5 models to more diverse communities that lack symmetry (Chesson 2000), as in the case of
6 intransitive competition. Intransitivity is defined as a cyclic ranking of species' competitive
7 ability, where no pair coexists but there is no strict competitive hierarchy. In our three-species
8 setting, intransitivity is equivalent to a rock-paper-scissors configuration. Just as MCT does not
9 incorporate non-hierarchical competition, existing studies of intransitivity do not consider cases
10 of pairwise coexistence or founder control. Our framework extends MCT to three-species
11 competition using three quantities: absolute fitness differences, pairwise niche overlap and
12 cyclic asymmetry, which quantifies the potential for intransitivity. Together these quantities
13 determine the outcome of three-species competition.

14
15
16 405 Among the three quantities determining competition outcomes, only low pairwise niche
17 overlap stabilizes the entire community. Hyper niche-overlap ($\rho > 1$) destabilizes the
18 community towards alternative stable states (Ke & Letten 2018). Large fitness differences tend
19 to result in the dominance of the species with the higher intrinsic growth rate, and
20 counterintuitively, small relative fitness differences can promote heteroclinic cycles. Increasing
21 cyclic asymmetry expands the parameter region where heteroclinic cycles are possible.

22
23
24 411 Intransitivity has often been thought of as a diversity-promoting force (Soliveres & Allan,
25 2018). In our three-species model, intransitivity occurs in the region between pairwise
26 coexistence regions in feasibility plots, shown with dashed triangles in Fig. 3ce. As seen in the
27 corresponding outcome plots, intransitivity sometimes leads to stable coexistence, but can also

1
2
3 415 result in heteroclinic cycles where species reach arbitrarily low densities (Fig. 4a) and would go
4
5 416 extinct in the real world (May & Leonard 1975). In fact, this is always the case in the absence of
6
7 417 niche differences ($\rho = 1$ in Figs. 5, S1). Therefore, intransitivity does not allow three-species
8
9 418 coexistence by itself, but can interact with niche differences to expand the size of the
10
11 419 coexistence region (Figs. 5, 6). However, note that in contrast to our well-mixed system, in
12
13 420 spatially extended systems, heteroclinic cycles can be stabilized through asynchronous
14
15 421 fluctuations that prevent global extinction (Kerr et al. 2002; Laird & Schamp 2006).
16
17
18
19
20
21 422 Since large fitness differences, high niche overlap and cyclic asymmetry all destabilize
22
23 423 three-species communities, three-species coexistence only occurs in a limited proportion of
24
25 424 environments in the model. Similar results can be seen across a range of empirical and
26
27 425 theoretical work where communities only consist of a subset of the species pool (May, 1973;
28
29 426 Medeiros et al., 2021; Song & Saavedra, 2018). Typically, regional species pools are fairly large
30
31 427 and the assembly process eliminates some species, resulting in a sub-community.
32
33
34
35 428 Mathematically, this is an example of the ‘curse of dimensionality’. For all species to coexist in a
36
37 429 high-dimensional system like a diverse community, every species has to be stabilized by the
38
39 430 processes acting in the system. In contrast, destabilization in any of these species result in
40
41 431 destabilization of the entire community.
42
43
44
45
46
47 432 By building on pairwise models and characterizing three-species competitive outcomes,
48
49 433 our work naturally invites the question “what next?” The importance of intransitivity could be
50
51 434 studied by measuring cyclic asymmetry in addition to fitness differences and pairwise niche
52
53 435 overlap in natural communities. Godoy et al. 2017 found that intransitivity was uncommon in
54
55
56
57
58
59
60

1
2
3 436 annual plant communities. Alternatively, resource-competition models could be used to
4
5 437 illuminate the ecological mechanisms that lead to competitive asymmetry and intransitivity
6
7 438 (Huisman & Weissing 1999).
8
9

10
11 439 One avenue for theoretical exploration would be the extension to predator-prey and
12
13 440 mutualistic interactions (see Bomze 1985, 1993 for a catalog of outcomes in the general two-
14
15 species Lotka-Volterra model). Concerning diversity, incrementally increasing community size is
16
17 441 clearly not a sustainable approach to understanding coexistence, since model complexity
18
19 increases too fast for complete analysis to be feasible. However, the transition from two to
20
21 443 three species is unique, since it involves the addition of indirect effects (Appendix F) that results
22
23 444 in a fundamentally different ecological process: intransitivity. Understanding three-species
24
25 competition also allows us to use triplets instead of pairs as a unit while investigating diverse
26
27 446 communities in the future. This gives us additional explanatory power by accounting for
28
29 447 intransitive competition. Finally, a range of other notable approaches to investigate coexistence
30
31 448 of diverse communities exist: focusing on networks of species (Allesina & Levine 2011; Allesina
32
33 449 & Tang, 2012, 2015; May, 1973), permanence of large communities (Hofbauer & Schreiber,
34
35 450 2022; Patel & Schreiber, 2018), trait-based approaches (Klausmeier et al., 2020), and
36
37 451 techniques inspired by statistical mechanics (Advani et al., 2018; Barbier et al., 2018). Fruitfully
38
39 452 combining these theoretical approaches with empirical work will help reduce the complexity to
40
41 453 manageable levels, thus advancing the research program into coexistence.
42
43
44
45
46
47
48
49
50
51
52
53
54
55
56
57
58
59
60

1
2
3 455 Acknowledgments
4
5

6 456 We thank three reviewers for useful comments on the manuscript, Mathematica Stack
7
8 457 Exchange users (particularly Henrik Schumacher and Michael E2) for essential programming
9
10 458 advice, and Elena Litchman for years of snark about this project. RR acknowledges support by
11
12 459 the HIFMB, a collaboration between the Alfred-Wegener-Institute, Helmholtz-Center for Polar
13
14 460 and Marine Research and the Carl-von-Ossietzky University Oldenburg, initially funded by the
15
16 461 Ministry of Science and Culture of Lower Saxony (MWK) and the Volkswagen Foundation
17
18 462 through the 'Niedersächsisches Vorab' grant program (ZN3285). CAK acknowledges funding
19
20 463 from the NSF (EF 2124800) and iDiv via the German Research Foundation (DFG FZT 118,
21
22 464 202548816), specifically funding through sDiv, the Synthesis Centre of iDiv. This is W. K. Kellogg
23
24 465 Biological Station contribution TBD.
25
26
27
28
29
30
31
32
33
34
35
36
37
38
39
40
41
42
43
44
45
46
47
48
49
50
51
52
53
54
55
56
57
58
59
60

For Review Only

1
2
3 466 **References**

- 4
5
6 467 Advani, M., Bunin, G., & Mehta, P. (2018). Statistical physics of community ecology: A cavity
7
8 468 solution to MacArthur's consumer resource model. *Journal of Statistical Mechanics: Theory and Experiment*, 2018(3), 033406. <https://doi.org/10.1088/1742-5468/aab04e>
- 9
10
11 469 Allesina, S., & Levine, J. M. (2011). A competitive network theory of species diversity.
12
13
14 470 Allesina, S., & Tang, S. (2012). Stability criteria for complex ecosystems. *Nature*, 483(7388),
15
16
17 471 *Proceedings of the National Academy of Sciences*, 108(14), 5638–5642.
18
19 472 <https://doi.org/10.1073/pnas.1014428108>
- 20
21
22 473 Allesina, S., & Tang, S. (2015). The stability–complexity relationship at age 40: A random matrix
23
24 474 perspective. *Population Ecology*, 57(1), 63–75. <https://doi.org/10.1007/s10144-014-0471-0>
- 25
26
27
28 475 Allesina, S., & Tang, S. (2015). The stability–complexity relationship at age 40: A random matrix
29
30 476 perspective. *Population Ecology*, 57(1), 63–75. <https://doi.org/10.1007/s10144-014-0471-0>
- 31
32
33 477 Armstrong, R. A., & McGehee, R. (1976). Coexistence of species competing for shared
34
35 478 resources. *Theoretical Population Biology*, 9(3), 317–328.
- 36
37
38 480 Barabás, G., D'Andrea, R., & Stump, S. M. (2018). Chesson's coexistence theory. *Ecological
39
40 481 Monographs*, 88(3), 277–303. <https://doi.org/10.1002/ecm.1302>
- 41
42
43 482 Barbier, M., Arnoldi, J.-F., Bunin, G., & Loreau, M. (2018). Generic assembly patterns in complex
44
45 483 ecological communities. *Proceedings of the National Academy of Sciences*, 115(9), 2156–
46
47 484 2161. <https://doi.org/10.1073/pnas.1710352115>
- 48
49
50 485 Bomze IM (1983) Lotka-Volterra equation and replicator dynamics: A two-dimensional
51
52 486 classification. *Biological Cybernetics*, 48, 201–211.
- 53
54
55
56
57
58
59
60

- 1
2
3 487 Bomze IM (1995) Lotka-Volterra equation and replicator dynamics: new issues in classification.
4
5 488 *Biological Cybernetics*, 72, 447–453.
6
7 489 Cenci, S., & Saavedra, S. (2018). Structural stability of nonlinear population dynamics. *Physical*
8
9 490 *Review E*, 97(1), 012401. <https://doi.org/10.1103/PhysRevE.97.012401>
10
11 491 Chang, C.-Y., Bajić, D., Vila, J. C. C., Estrela, S., & Sanchez, A. (2023). Emergent coexistence in
12
13 492 multispecies microbial communities. *Science*, 381(6655), 343–348.
14
15 493 <https://doi.org/10.1126/science.adg0727>
16
17 494 Chesson, P. (1990). MacArthur's consumer-resource model. *Theoretical Population Biology*, 37,
18
19 495 26–38.
20
21 496 Chesson, P. (2000). Mechanisms of maintenance of species diversity. *Annual Review of Ecology*
22
23 497 and Systematics, 343–366.
24
25 498 Chesson, P. (2018). Updates on mechanisms of maintenance of species diversity. *Journal of*
26
27 499 *Ecology*, 106(5), 1773–1794. <https://doi.org/10.1111/1365-2745.13035>
28
29 500 Chesson, P. (2020). Species coexistence. In K. S. McCann & G. Gellner (Eds.), *Theoretical*
30
31 501 *ecology: Concepts and applications* (pp. 5–27). Oxford University Press.
32
33 502 <https://oxford.universitypressscholarship.com/view/10.1093/oso/9780198824282.001.0001/oso-9780198824282-chapter-11>
34
35 503
36
37 504 Gilpin, M. E. (1975). Limit cycles in competition communities. *The American Naturalist*,
38
39 505 109(965), 51–60. <https://doi.org/10.1086/282973>
40
41 506 Godoy, O., Stouffer, D. B., Kraft, N. J. B., & Levine, J. M. (2017). Intransitivity is infrequent and
42
43 507 fails to promote annual plant coexistence without pairwise niche differences. *Ecology*,
44
45 508 98(5), 1193–1200. <https://doi.org/10.1002/ecy.1782>

- 1
2
3 509 Hofbauer, J. (1994). Heteroclinic cycles in ecological differential equations. *Tatra Mountains*
4
5 510 *Mathematical Publications*, 4, 105–116.
6
7 511 Hofbauer, J., & Schreiber, S. J. (2022). Permanence via invasion graphs: Incorporating
8 community assembly into modern coexistence theory. *Journal of Mathematical Biology*,
9
10 512 85(5), 54. <https://doi.org/10.1007/s00285-022-01815-2>
11
12 513
13
14 514 Hofbauer, J., & Sigmund, K. (1998). *Evolutionary Games and Population Dynamics*. Cambridge
15 University Press. <https://www.journals.uchicago.edu/doi/10.1086/393199>
16
17 515
18
19 516 Hofbauer, J., & So, J. W.-H. (1994). Multiple limit cycles for three dimensional Lotka-Volterra
20 equations. *Applied Mathematics Letters*, 7(6), 65–70. <https://doi.org/10.1016/0893->
21
22 517
23
24 518 9659(94)90095-7
25
26
27 519 Huisman, J., & Weissing, F. J. (1999) Biodiversity of plankton by species oscillations and chaos.
28
29 520 *Nature* 402, 407–410.
30
31
32 521 Ke, P.-J., & Letten, A. D. (2018). Coexistence theory and the frequency-dependence of priority
33 effects. *Nature Ecology & Evolution*, 2, 1691–1695. <https://doi.org/10.1038/s41559-018->
34
35 522
36
37 523 0679-z
38
39
40 524 Kerr, B., Riley, M. A., Feldman, M. W., & Bohannan, B. J. M. (2002). Local dispersal promotes
41 biodiversity in a real-life game of rock–paper–scissors. *Nature*, 418(6894), 171–174.
42
43 525
44
45 526 <https://doi.org/10.1038/nature00823>
46
47 527 Klimentko, A. (2015). Intransitivity in theory and in the real world. *Entropy*, 17(12), 4364–4412.
48
49 528 <https://doi.org/10.3390/e17064364>
50
51
52 529 Laird, R. A., & Schamp, B. S. (2006). Competitive intransitivity promotes species coexistence.
53
54
55 530 *American Naturalist*, 168(2), 182–193.
56
57
58
59
60

- 1
2
3 531 May, R. M. (1973). *Stability and complexity in model ecosystems*. Princeton University Press.
4
5 532 May, R. M., & Leonard, W. J. (1975). Nonlinear aspects of competition between three species.
6
7 533 *SIAM Journal of Applied Mathematics*, 29(2), 243–253.
8
9
10 534 Medeiros, L. P., Boege, K., del-Val, E., Zaldívar-Riverón, A., & Saavedra, S. (2021). Observed
11 ecological communities are formed by species combinations that are among the most
12 likely to persist under changing environments. *The American Naturalist*, 197(1), E17–
13
14 536 E29. <https://doi.org/10.1086/711663>
15
16
17
18 537 Patel, S., & Schreiber, S. J. (2018). Robust permanence for ecological equations with internal
19 and external feedbacks. *Journal of Mathematical Biology*, 77(1), 79–105.
20
21 539 <https://doi.org/10.1007/s00285-017-1187-5>
22
23
24 540 Saavedra, S., Rohr, R. P., Bascompte, J., Godoy, O., Kraft, N. J., & Levine, J. M. (2017). A
25 structural approach for understanding multispecies coexistence. *Ecological
26 Monographs*, 87(3), 470–486.
27
28
29 541 Soliveres, S., & Allan, E. (2018). Everything you always wanted to know about intransitive
30 competition but were afraid to ask. *Journal of Ecology*, 106(3), 807–814.
31
32 542 <https://doi.org/10.1111/1365-2745.12972>
33
34
35 543 Song, C., & Saavedra, S. (2018). Will a small randomly assembled community be feasible and
36 stable? *Ecology*, 99(3), 743–751. <https://doi.org/10.1002/ecy.2125>
37
38
39 544 Tilman, D. (1985). The resource-ratio hypothesis of plant succession. *The American Naturalist*,
40 125(6), 827–852. <https://doi.org/10.1086/284382>
41
42
43
44
45
46
47
48
49
50
51
52
53
54
55
56
57
58
59
60

Figure Legends

Figure 1. Color coding for the 23 different outcomes of three-species Lotka Volterra competition. Monocultures are represented by primary colors and coexisting pairs are shown by mixing the constituent species' colors. Alternative stable states are shown as stripes corresponding to colors of the constituent stable states. Dark gray represents the coexistence of all three species. Heteroclinic cycles are shown as spirals and white space represents limit cycles.

Figure 2. The effect of pairwise coexistence versus founder control on the outcome of competition. The left column shows the feasibility regions for the pairwise equilibria and their stability (stable in orange, unstable in lavender) and feasibility regions for the three-species equilibrium (grey). The right column shows the corresponding competitive outcomes. The legend for the different colors for outcomes is shown in Fig. 1 and the parameter values are provided in Appendix E. **(a)-(b)** All pairs coexist. **(c)-(d)** two pairs coexist, one pair shows founder control. **(e)-(f)** One pair coexists, two pairs show founder control. **(g)-(h)** All pairs show founder control.

Figure 3. The effect of cyclic asymmetry on the outcome of competition. The left column shows the feasibility regions for the pairwise equilibria and feasibility regions for the three-species equilibrium (grey). The right column shows the corresponding competitive outcomes. All pairs have identical niche overlap $\rho = 0.5$. The legend for the different colors for outcomes is shown in Fig. 1 and the parameter values are provided in Appendix E. **(a)-(b)** When there is no cyclic asymmetry ($\bar{A} = 1$), the pairwise stability regions and the regions with different outcomes are all symmetrical. The central region where the three-species equilibrium is feasible (dark gray in A) leads to stable coexistence of all three species (dark gray in B). **(c)-(d)** At intermediate levels of cyclic asymmetry ($\bar{A} = 3$), the pairwise stability regions are twisted. This gives rise to a range of parameters in the center of C where the three-species equilibrium is stable but all pairwise equilibria are not feasible (bounded by a dashed line). However, the competitive outcome continues to be a stable three-species equilibrium (dark gray region in D). **(e)-(f)** At high levels of cyclic asymmetry ($\bar{A} = 4$), the parameter region where the three-species equilibrium is stable but all pairwise equilibria are not becomes larger (central region in E). The competitive outcome at the center of unit simplex switches to a mix of heteroclinic cycles (spirals), limit cycles (white) and stable three-species (dark gray) equilibrium.

Figure 4. Population dynamics for three cases from Fig. 3. **(a)** A heteroclinic cycle. **(b)** A limit cycle. **(c)** A stable equilibrium. Parameter values are provided in Appendix E.

Figure 5. Competitive outcome as niche overlap, cyclic asymmetry and absolute fitnesses vary. The x-axis represents pairwise niche overlap, which is assumed to be the same for all three pairs. Niche overlap goes from very low (pairs can coexist) on the left to very high on the right (pairs can show founder control). The y-axis represents cyclic asymmetry in the triplet, which goes from non-existent to high. The legend for the different colors for outcomes is shown in Fig. 1 and the parameter values are provided in Appendix E. Low niche overlap (bottom left corner)

1
2
3 590 in the pairs stabilizes the community, leading to three-species coexistence. High niche overlap
4 591 (bottom right corner) in the pairs leads to alternative stable states. Cyclic asymmetry, when
5 592 combined with niche overlaps close to 1, destabilizes the community and leads to heteroclinic
6 593 cycles.
7
8

9 594 **Figure 6.** The interactive effect of pairwise niche overlap and cyclic asymmetry on the
10 595 probability of three-species coexistence (the proportion of environments in the unit simplex
11 596 $r_1 + r_2 + r_3 = 1$ resulting in three-species coexistence). Warmer colors represent higher
12 597 proportions of environments resulting in three-species coexistence.
13
14

15 598 **Figure S1.** The outcome of competition for symmetric species ($r_1 = r_2 = r_3 = 1$) with equal
16 599 niche overlap $\rho_{12} = \rho_{23} = \rho_{13} = \rho$ and cyclic asymmetry $A_{12} = A_{23} = A_{31} = \bar{A}$, comparable
17 600 with Fig. 1 of May & Leonard (1975). Gray region = stable three-species coexistence, spirals =
18 601 heteroclinic cycle, stripes = three-way founder control.
19
20

21 602 **Figure S2.** Three-species competition outcomes as niche overlap, cyclic asymmetry and fitness
22 603 imbalance are varied, when the niche overlap of one pair is the reciprocal of the other two
23 604 ($\rho_{12} = \rho_{23} = 1/\rho_{31}$). The x-axis represents pairwise niche overlap, which goes from very low
24 605 (pairs can coexist) on the left to very high on the right (pairs can show founder control). The y-
25 606 axis represents cyclic asymmetry in the triplet, which goes from non-existent ($\bar{A} = 1$) to high
26 607 ($\bar{A} = 8$). Each unit simplex shows the competitive outcome at a combination of niche overlap
27 608 and cyclic asymmetry and moving within the unit simplex changes the fitness imbalance.
28
29 Different colors represent different competitive outcomes, and a legend is provided in Fig. 1.
30 The inequality of pairwise niche overlaps breaks the symmetry between the regions. At high
31 610 cyclic asymmetry, low niche overlap (top left corner) counteracts the cyclic asymmetry, leading
32 611 to a relatively larger region of three-species coexistence and only a small region of heteroclinic
33 612 cycles. High niche overlap (bottom right corner) at high cyclic asymmetry also influences the
34 613 competition outcome and leads to alternative stable states.
35
36

37 615 **Figure S3.** Recentering in the case of unequal competitive asymmetry. The left column shows
38 616 the feasibility regions for the pairwise equilibria and feasibility regions for the three-species
39 617 equilibrium (grey). The right column shows the corresponding competitive outcomes. **(a)-(b)**
40 618 The uncentered unit simplex. **(c)-(d)** Recentered using eqn. (12). **(e)-(f)** The comparable case
41 619 with equal $A_{ij} = \bar{A}$. The legend for the different colors for outcomes is shown in Fig. 1.
42 Parameter values: **(a)-(d)** $\rho = 0.5, A_{12} = 16, A_{23} = 2, A_{31} = 0.25, \bar{A} = 2$ or in terms of the
43 620 competition coefficients, $\alpha = \{\{1, 0.03125, 0.125\}, \{8, 1, 0.25\}, \{2, 1, 1\}\}$. **(e)-(f)** $\rho = 0.5, A_{12} =$
44 621 $A_{23} = A_{31} = \bar{A} = 2$, or $\alpha = \{\{1, 0.25, 1\}, \{1, 1, 0.25\}, \{0.25, 1, 1\}\}$.
45
46

47 623 **Figure S4.** Recentering in the case of unequal competitive asymmetry. The left column shows
48 624 the feasibility regions for the pairwise equilibria and feasibility regions for the three-species
49 625 equilibrium (grey). The right column shows the corresponding competitive outcomes. **(a)-(b)**
50 626 The uncentered unit simplex. **(c)-(d)** Recentered using eqn. (12). **(e)-(f)** The comparable case
51 627 with equal $A_{ij} = \bar{A}$. The legend for the different colors for outcomes is shown in Fig. 1.
52 Parameter values: **(a)-(d)** $\rho = 0.5, A_{12} = 32, A_{23} = 4, A_{31} = 0.5, \bar{A} = 4$ or in terms of the
53
54

1
2
3 629 competition coefficients, $\alpha = \{\{1,0.015625,0.25\}, \{16,1,0.125\}, \{1,2,1\}\}$. (e)-(f) $\rho = 0.5, A_{12} =$
4 630 $A_{23} = A_{31} = \bar{A} = 4$, or $\alpha = \{\{1,0.125,2\}, \{2,1,0.125\}, \{0.125,2,1\}\}$.
5 631
6 632
7 633
8 634
9 635
10 636
11 637
12
13
14

Figure S5. Population dynamics for three cases from Fig. S4d. (a) A stable three-species equilibrium and (b) a heteroclinic cycle for different initial conditions ($\{N_1, N_2, N_3\} = \{0.0266667, 0.213333, 0.213333\}$ and $\{N_1, N_2, N_3\} = \{0.0001, 0.0001, 0.0001\}$ respectively). Other parameters: $\{r_1, r_2, r_3\} = \{1/12, 2/3, 2/3\}$, corresponding to the center of the gray/spiral region of Fig. S4D. (c) A limit cycle with $\{r_1, r_2, r_3\} = \{0.081, 1.024, 0.326\}$, corresponding to the white region of Fig. S4d.

For Review Only

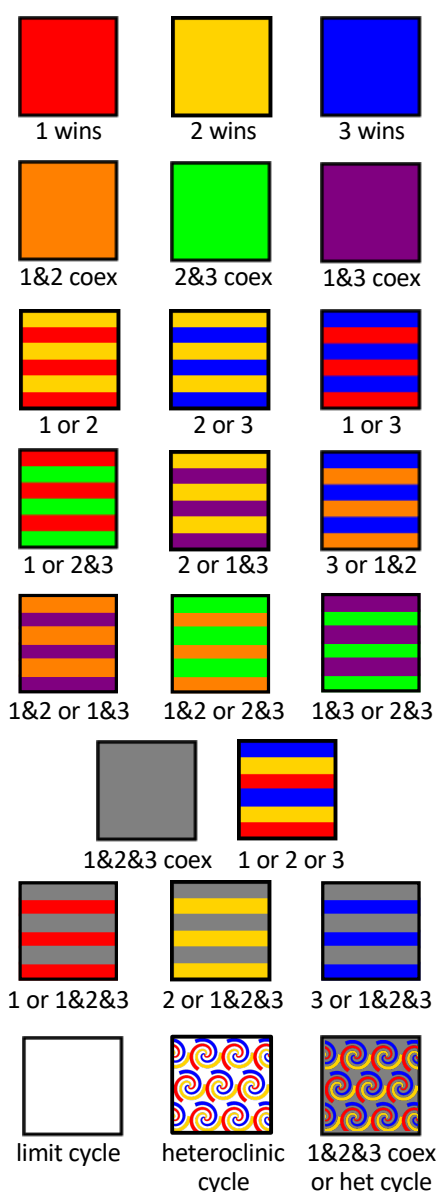


Figure 1

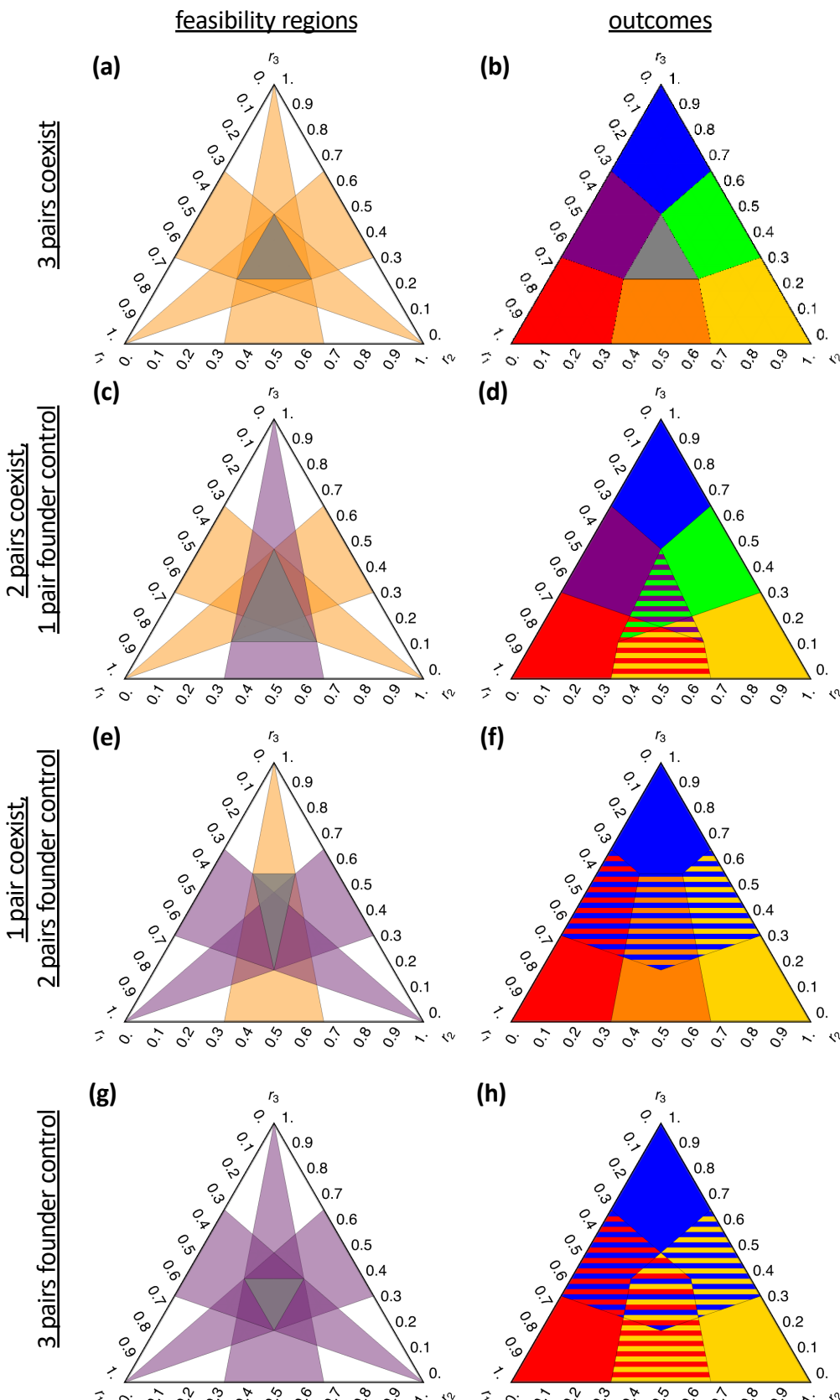


Figure 2

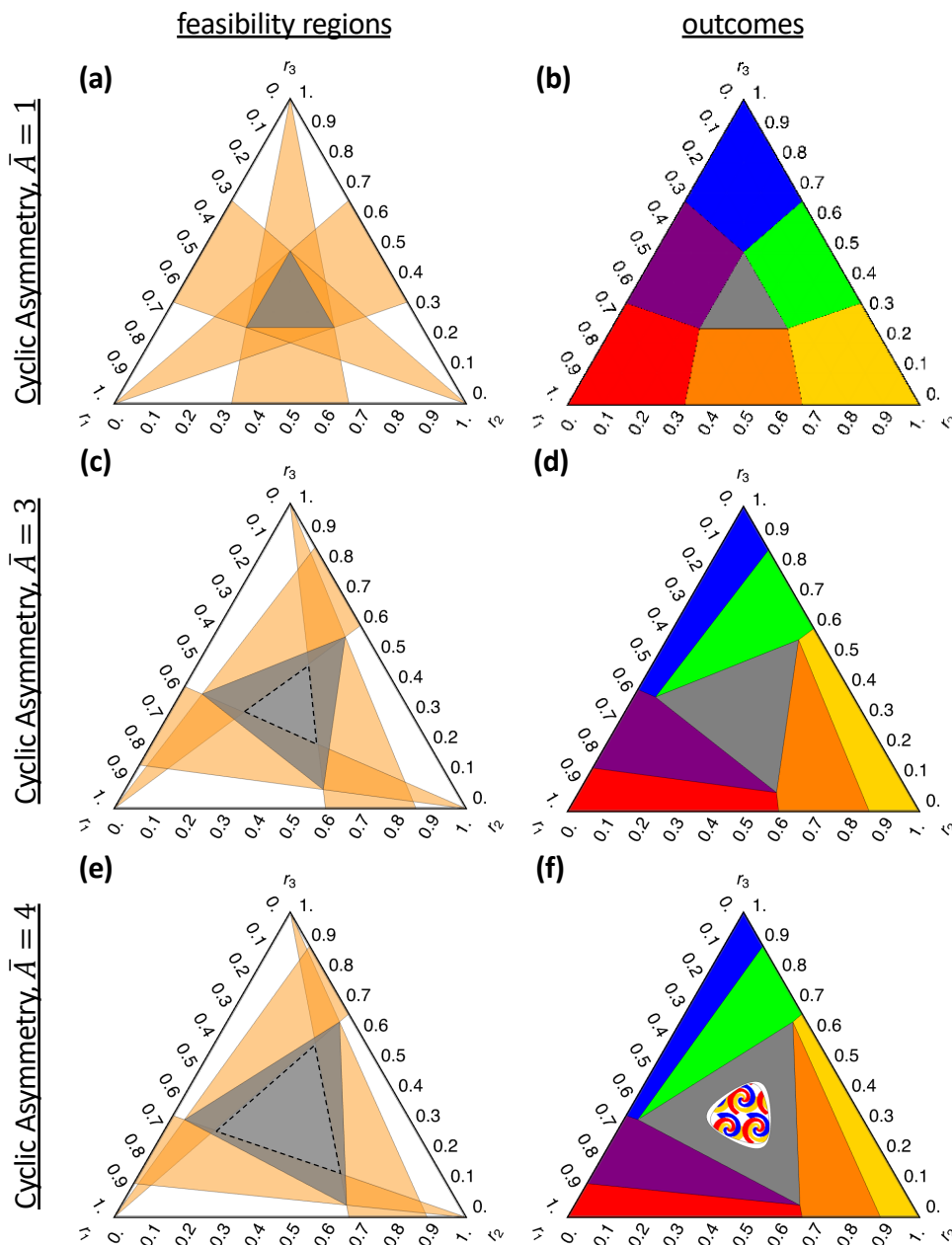


Figure 3

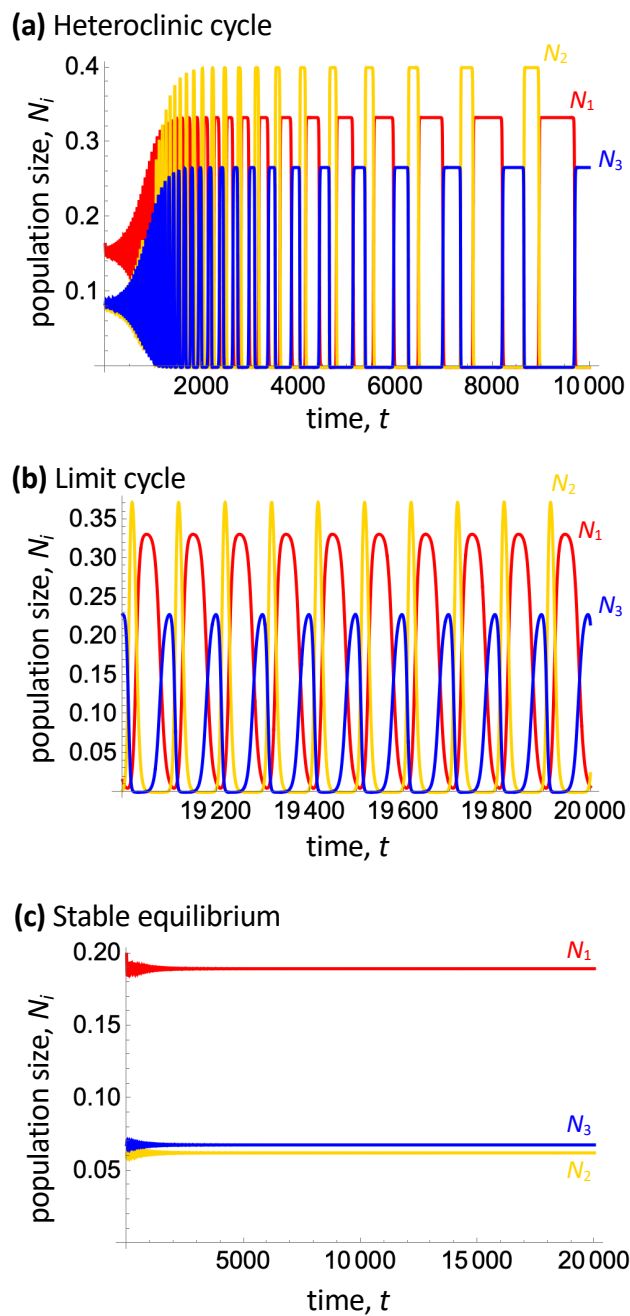


Figure 4

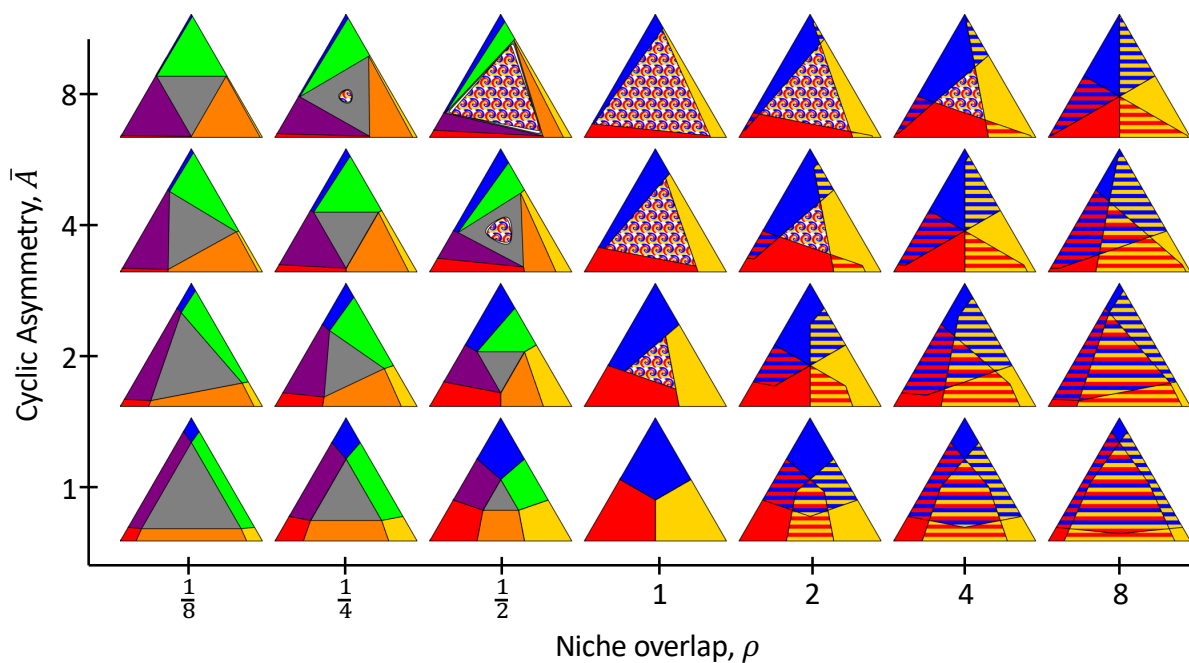


Figure 5

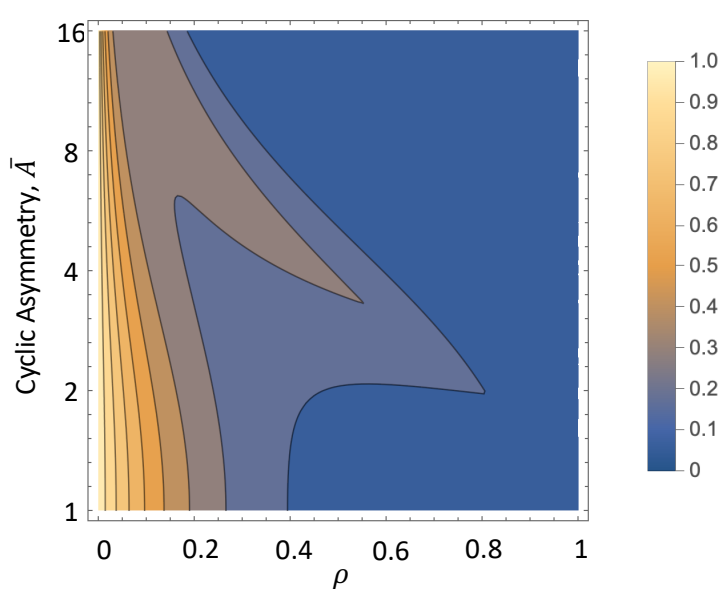


Figure 6

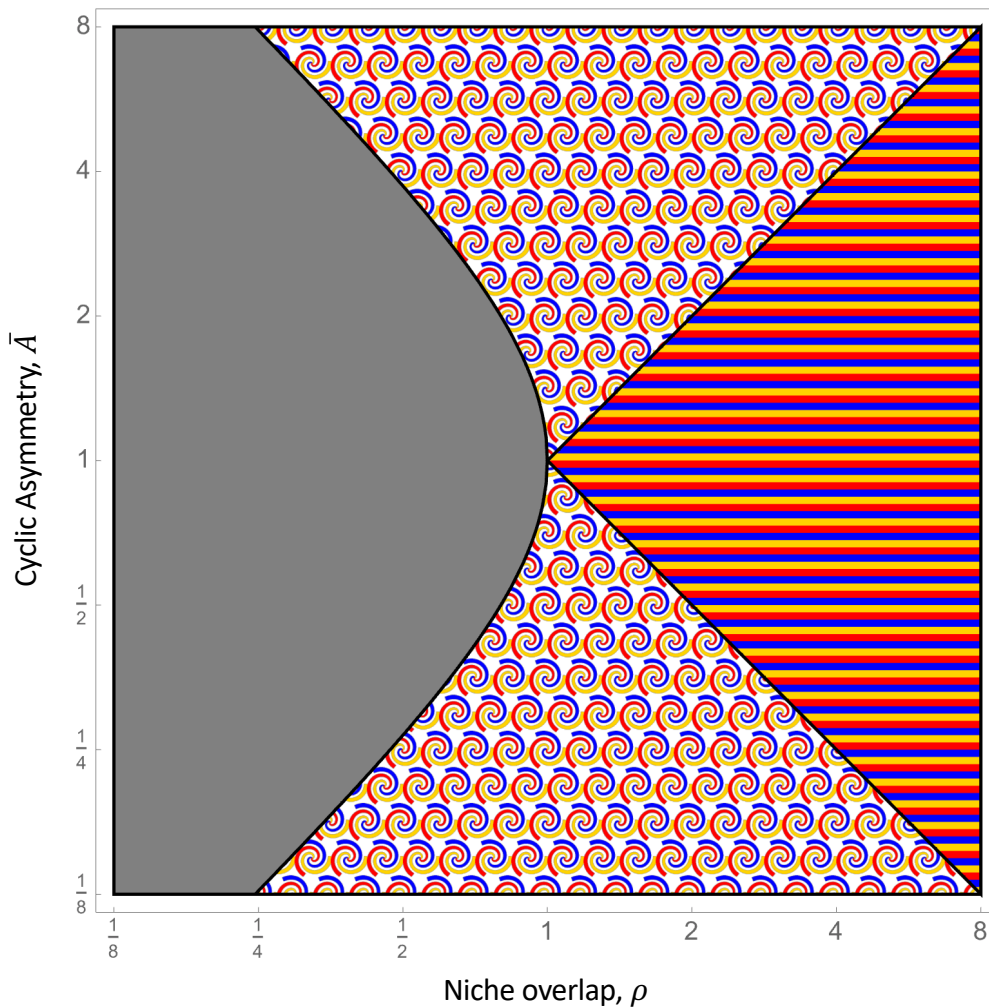


Fig. S1

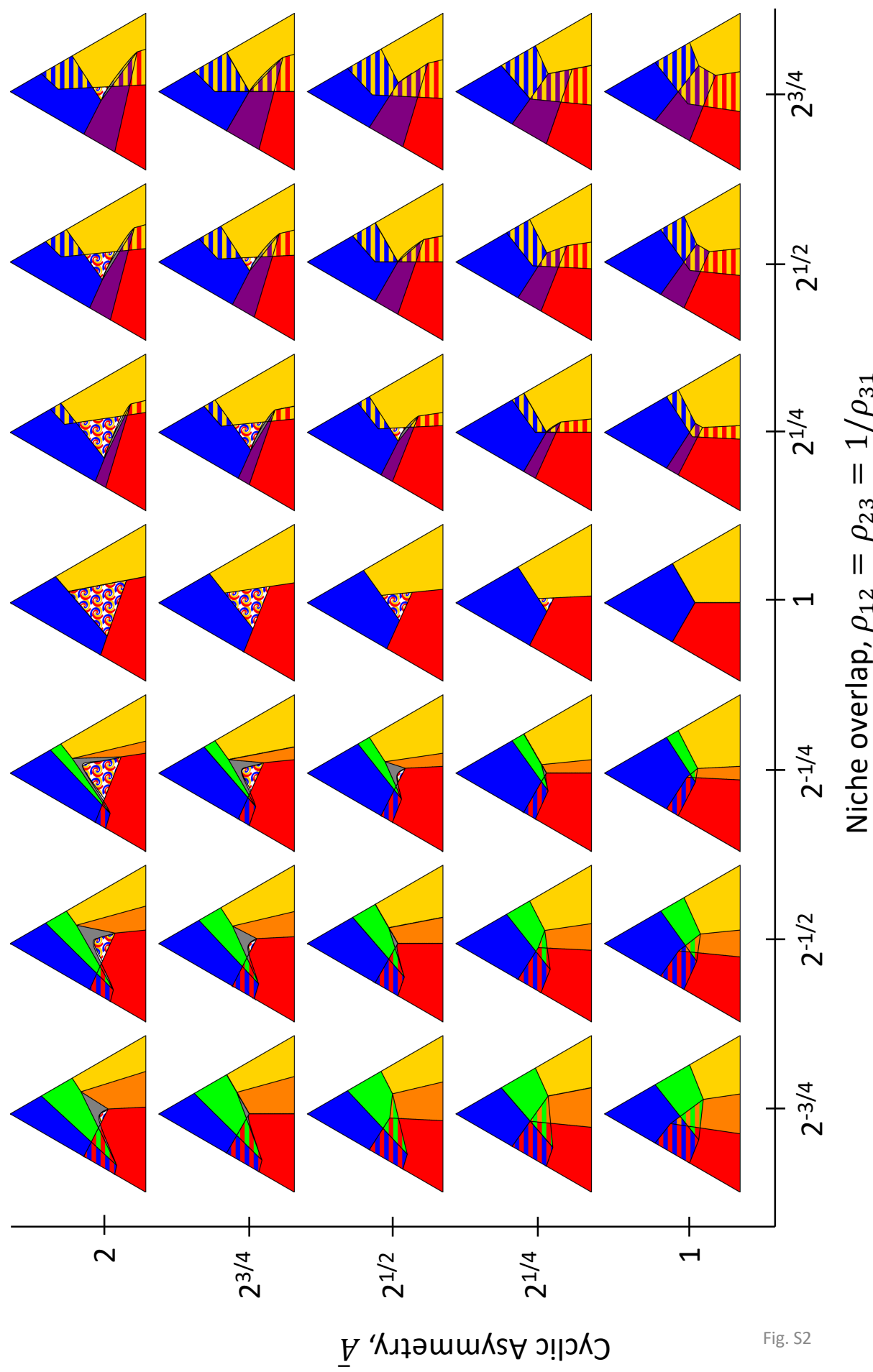


Fig. S2

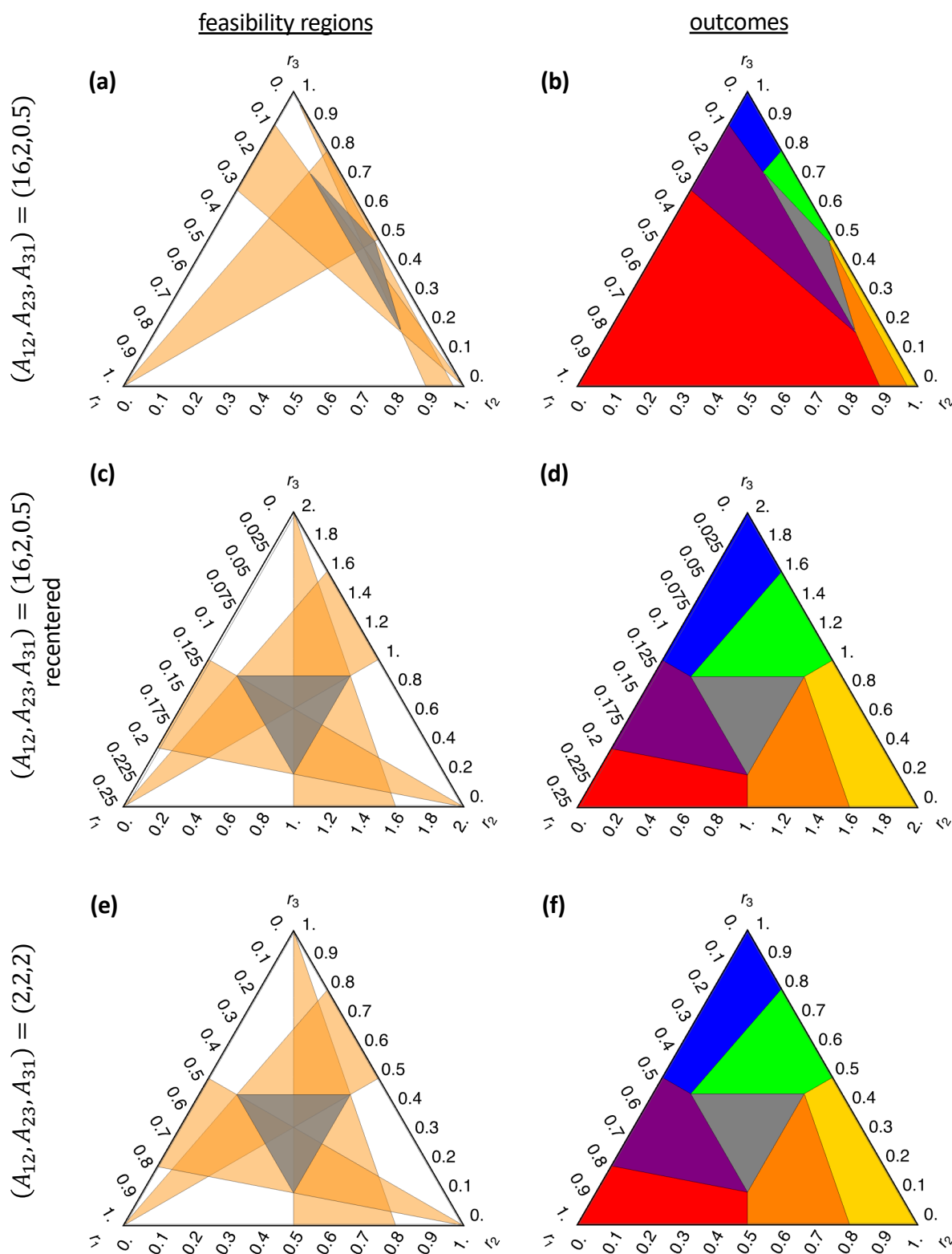
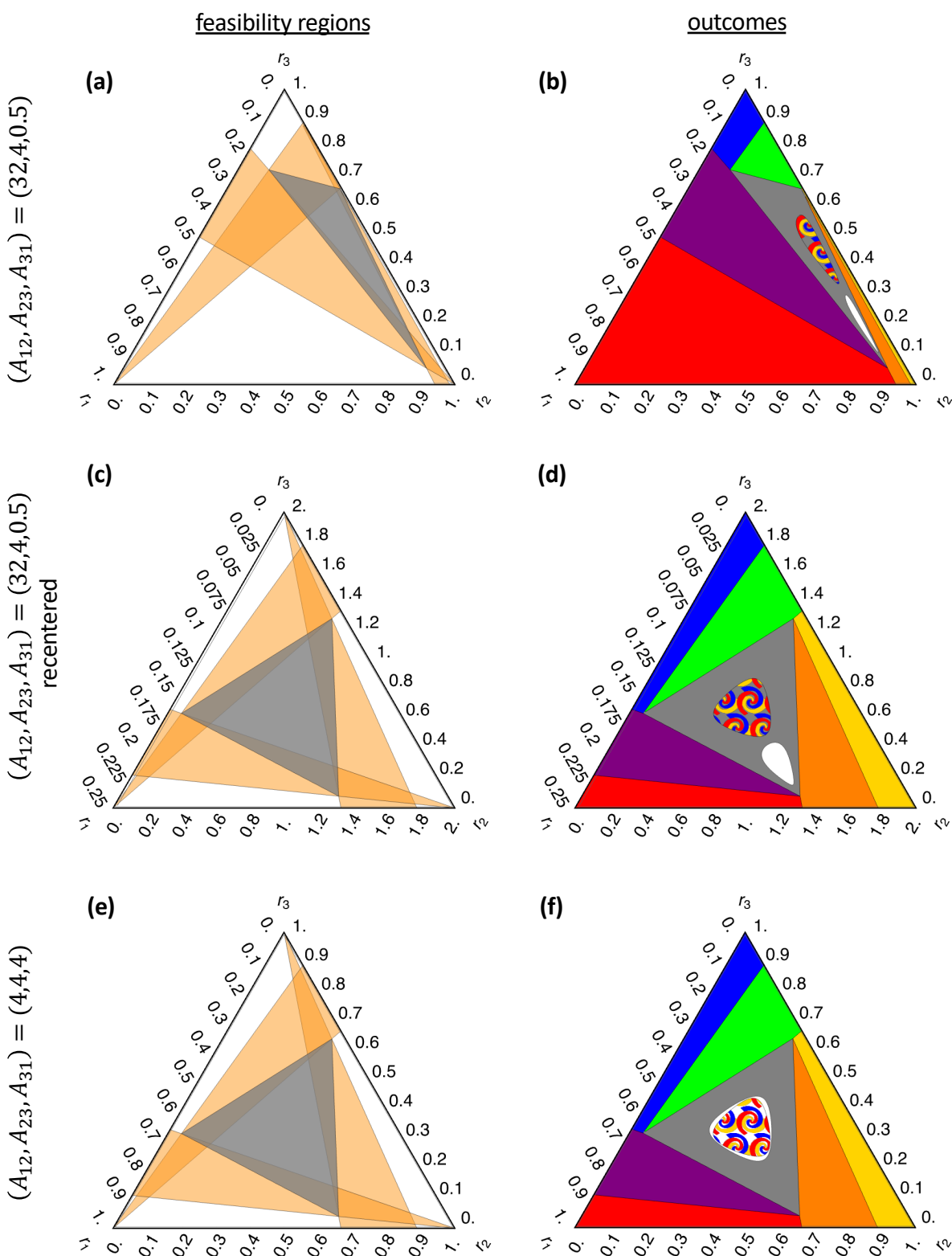


Fig. S3



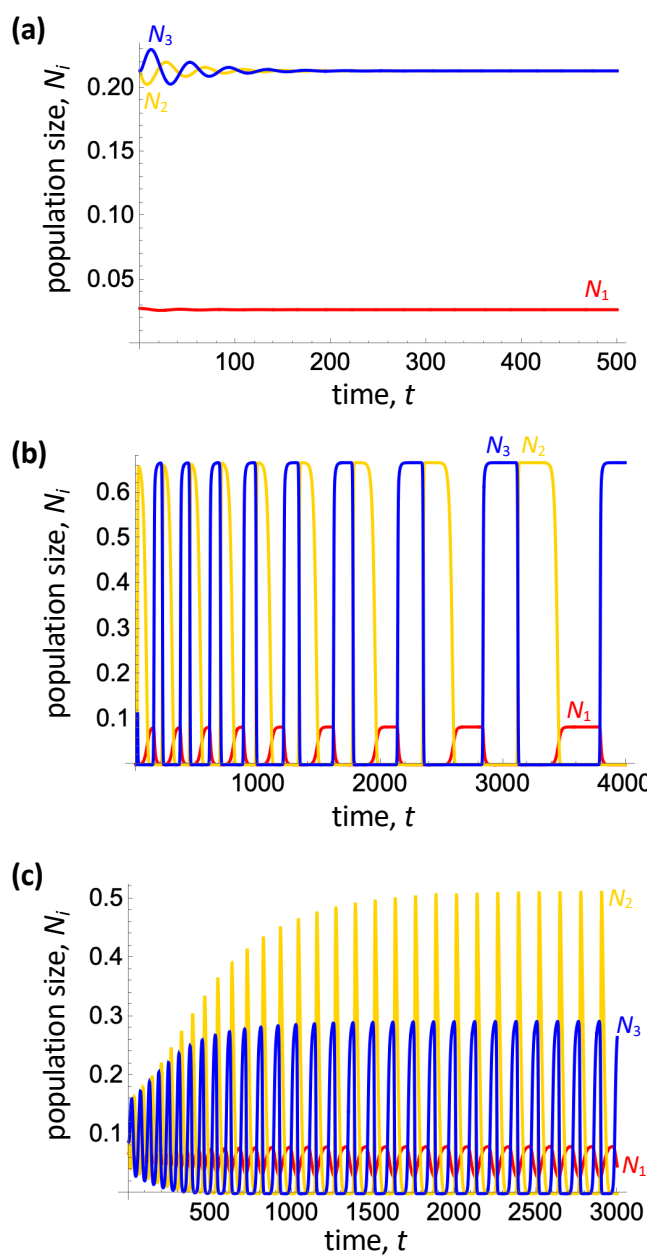


Fig. S5

1
2
3 Appendices
4
5

6 A: Constructing outcome plots
7
8

9 B: Constructing and reading a feasibility plot
10
11

12 C: Reading feasibility and outcome plots together
13
14

15 D: Nondimensionalization
16
17

18 E: Parameter values for figures
19
20

21 F: Inverse competition matrix exploration
22
23
24
25
26
27
28
29
30
31
32
33
34
35
36
37
38
39
40
41
42
43
44
45
46
47
48
49
50
51
52
53
54
55
56
57
58
59
60

For Review Only

Appendix A: Constructing Outcome Plots

Details of Analysis

To determine the outcome of three-species competition (Eqn. A1), we use a combination of feasibility analysis, invasion analysis, and dynamical stability analysis.

$$\frac{dN_1}{dt} = (r_1 - \alpha_{11}N_1 - \alpha_{12}N_2 - \alpha_{13}N_3)N_1 \quad (\text{A1a})$$

$$\frac{dN_2}{dt} = (r_2 - \alpha_{21}N_1 - \alpha_{22}N_2 - \alpha_{23}N_3)N_2 \quad (\text{A1b})$$

$$\frac{dN_3}{dt} = (r_3 - \alpha_{31}N_1 - \alpha_{32}N_2 - \alpha_{33}N_3)N_3 \quad (\text{A1c})$$

By setting each of Eqn. A1 equal to zero, we see that each species either has zero per capita growth rate ($dN_i/(N_i dt) = 0$) or is absent ($\hat{N}_i = 0$). Therefore, because the per capita growth rate is a linear function of the densities, there are eight equilibria: the trivial zero-species equilibrium, three one-species equilibria, three two-species equilibria, and a unique three-species equilibrium. Other possible limit sets are limit cycles and a heteroclinic cycle connecting the one-species equilibria.

An equilibrium is *feasible* if all species have non-negative densities ($\hat{N}_i \geq 0$). This is the basis of the structural stability framework.

The invasion rate of absent species *inv* into resident community *res* is defined as its per capita growth when rare:

$$\lambda_{\text{inv},\text{res}} = \frac{1}{N_{\text{inv}}} \frac{dN_{\text{inv}}}{dt} \Big|_{\hat{N}_{\text{res}}} \quad (\text{A2})$$

An equilibrium is *invasive* by species *inv* if $\lambda_{\text{inv},\text{res}} > 0$ and is *uninvasive* if $\lambda_{\text{inv},\text{res}} < 0$ for all possible invaders. This is the basis of the modern coexistence framework.

An equilibrium is *dynamically stable* if the system returns to it after a small perturbation. An equilibrium is dynamically stable if all of the eigenvalues of the Jacobian matrix

$$J = \begin{bmatrix} \frac{\partial \left(\frac{dN_1}{dt} \right)}{\partial N_1} & \frac{\partial \left(\frac{dN_1}{dt} \right)}{\partial N_2} & \frac{\partial \left(\frac{dN_1}{dt} \right)}{\partial N_3} \\ \frac{\partial \left(\frac{dN_2}{dt} \right)}{\partial N_1} & \frac{\partial \left(\frac{dN_2}{dt} \right)}{\partial N_2} & \frac{\partial \left(\frac{dN_2}{dt} \right)}{\partial N_3} \\ \frac{\partial \left(\frac{dN_3}{dt} \right)}{\partial N_1} & \frac{\partial \left(\frac{dN_3}{dt} \right)}{\partial N_2} & \frac{\partial \left(\frac{dN_3}{dt} \right)}{\partial N_3} \end{bmatrix}_{N=\hat{N}} \quad (\text{A3})$$

have negative real parts. Invasion analysis is a special case of dynamical stability analysis that is more ecologically motivated and easier to calculate. A shortcut to determining stability are the Routh-Hurwitz criteria (Murata 1985).

A heteroclinic cycle $\{i\} \rightarrow \{j\} \rightarrow \{k\} \rightarrow \{i\}$ connects the three one-species equilibria. Its existence requires $\lambda_{j,i} > 0 > \lambda_{i,j}$, $\lambda_{k,j} > 0 > \lambda_{j,k}$, and $\lambda_{i,k} > 0 > \lambda_{k,i}$, so that there is an intransitive rock-paper-scissors cycle of invasibility. A heteroclinic cycle is dynamically stable if the product of the positive invasion rates is less than the negative product of the negative invasion rates (Hofbauer & Sigmund 1988; Hofbauer & So 1994):

$$\lambda_{j,i}\lambda_{k,j}\lambda_{i,k} < -\lambda_{i,j}\lambda_{j,k}\lambda_{k,i} \quad (\text{A4})$$

The existence of a limit cycle is difficult to characterize analytically, but occurs when no other equilibrium or heteroclinic cycle is stable. Its stability can be determined numerically using Floquet exponents (Klausmeier 2008) but here we rely on numerical simulation of Eqn. (A1). It is possible that limit cycles (stable or unstable) may exist under other conditions, but we did not encounter them in our explorations.

Table A1 summarizes the stability criteria of all of the possible equilibria of three-species LV competition. There are at least 23 possible outcomes of the three-species LV competition model, with many varieties of alternative stable states (Fig. 1). Table A2 gives the conditions for each of these outcomes based on the stability of equilibria. The supplemental Mathematica code simplifies these conditions and uses them for plotting outcome plots.

Table A1. Equilibria and their stability.

Equilibria	Stability Criteria
Zero species, {}: $\widehat{N}_1 = \widehat{N}_2 = \widehat{N}_3 = 0$	Unstable due to our assumption $r_i > 0$
One species, {i}: $\widehat{N}_i = \frac{r_{ii}}{\alpha_{ii}}$ $\widehat{N}_j = \widehat{N}_k = 0$	$\lambda_{j,i} < 0, \lambda_{k,i} < 0$ (uninvadable by <i>j</i> and <i>k</i>)
Two species, {i, j}: $\widehat{N}_i = \frac{r_i \alpha_{jj} - r_j \alpha_{ij}}{\alpha_{ii} \alpha_{jj} - \alpha_{ij} \alpha_{ji}}$ $\widehat{N}_j = \frac{r_j \alpha_{ii} - r_i \alpha_{ji}}{\alpha_{ii} \alpha_{jj} - \alpha_{ij} \alpha_{ji}}$ $\widehat{N}_k = 0$	$\lambda_{i,j} > 0, \lambda_{j,i} > 0$ (mutual invadability of <i>i</i> and <i>j</i> , implies feasibility) $\lambda_{k,ij} < 0$ (uninvadable by <i>k</i>)
Three species, {1, 2, 3}: $\widehat{\vec{N}} = \alpha^{-1} \vec{r}$	$\text{Tr}(J) < 0, \text{Det}(J) < 0, \begin{vmatrix} J_{11} + J_{22} & J_{23} & -J_{13} \\ J_{32} & J_{11} + J_{33} & J_{12} \\ -J_{31} & J_{21} & J_{22} + J_{33} \end{vmatrix} < 0$ (modified Routh-Hurwitz conditions; Murata 1985)
Heteroclinic cycle: $\{i\} \rightarrow \{j\} \rightarrow \{k\} \rightarrow \{i\}$	$\lambda_{j,i}\lambda_{k,j}\lambda_{i,k} < -\lambda_{i,j}\lambda_{j,k}\lambda_{k,i}$ (Hofbauer & Sigmund 1988; Hofbauer & So 1994)

Table A2. Outcomes and their conditions.

Outcome	Conditions
i wins	$\{i\}$ stable $\{j\}$ and $\{k\}$ unstable $\{j, k\}$ unstable or infeasible $\{1, 2, 3\}$ unstable or infeasible
$i \& j$ coexist	$\{i, j\}$ stable $\{k\}$ unstable $\{i, k\}$ and $\{j, k\}$ unstable or infeasible
i or j wins	$\{i\}$ and $\{j\}$ stable $\{k\}$ unstable
i wins or $j \& k$ coexist	$\{i\}$ and $\{j, k\}$ stable
$i \& j$ coexist or $i \& k$ coexist	$\{i, j\}$ and $\{i, k\}$ stable
i wins or $1 \& 2 \& 3$ coexist	$\{i\}$ and $\{1, 2, 3\}$ stable
$1 \& 2 \& 3$ coexist	$\{1, 2, 3\}$ stable $\{1\}, \{2\}$ and $\{3\}$ unstable $\{i\} \rightarrow \{j\} \rightarrow \{k\} \rightarrow \{i\}$ unstable
1 or 2 or 3 wins	$\{1\}, \{2\}$ and $\{3\}$ stable
heteroclinic cycle	$\{i\} \rightarrow \{j\} \rightarrow \{k\} \rightarrow \{i\}$ stable $\{1, 2, 3\}$ unstable
$1 \& 2 \& 3$ coexist or heteroclinic cycle	$\{i\} \rightarrow \{j\} \rightarrow \{k\} \rightarrow \{i\}$ stable $\{1, 2, 3\}$ stable
limit cycle	$\{i\} \rightarrow \{j\} \rightarrow \{k\} \rightarrow \{i\}$ unstable $\{1, 2, 3\}$ unstable

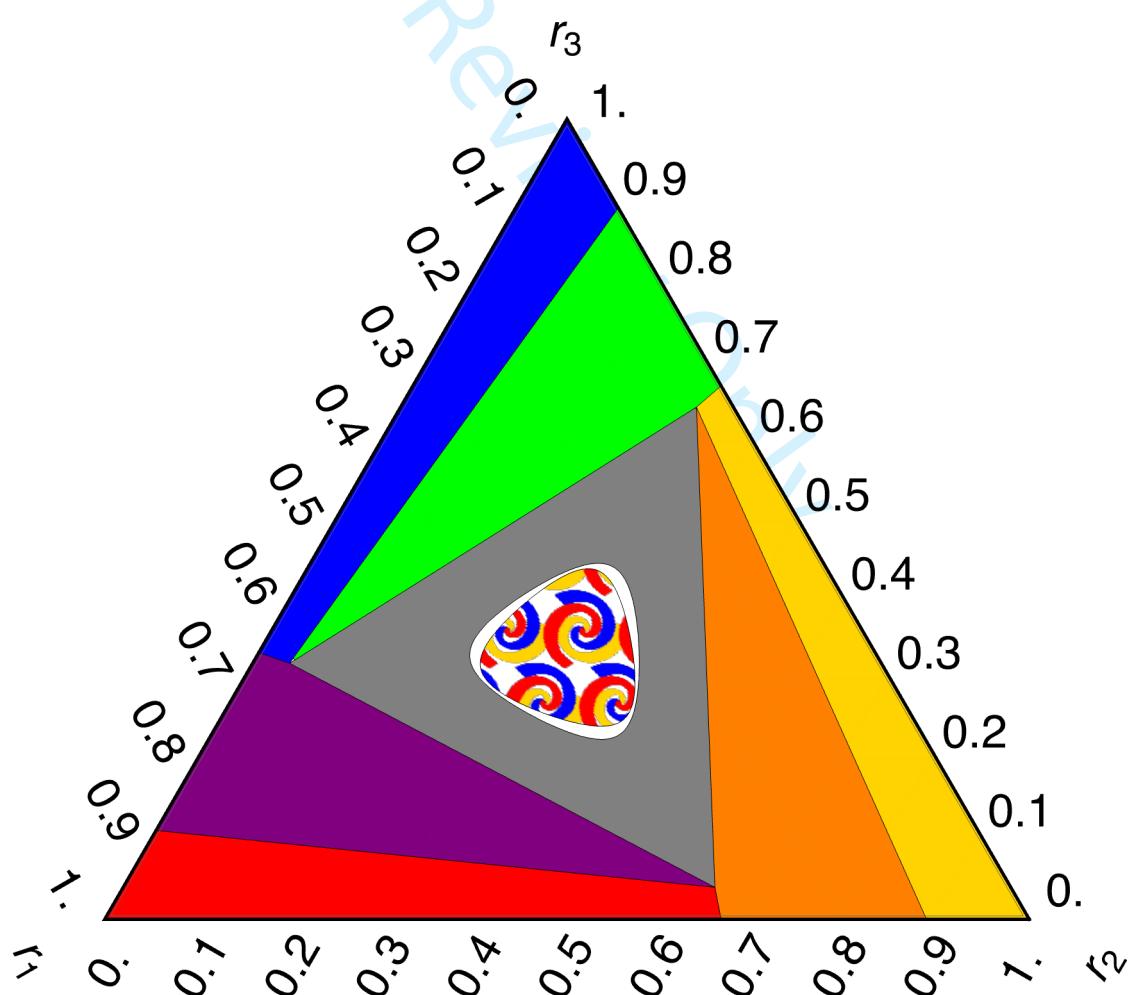
1
2
3 Numerical examples
4
5

6 To make the preceding analysis more concrete, we present numerical examples of the
7 eleven distinct outcomes we found in Table A2 below. For each of the eight equilibria, we
8 give the abundances and eigenvalues of the Jacobian matrix of feasible equilibria. The
9 outcomes (feasible and stable) are highlighted. We also calculate the stability of a
10 heteroclinic cycle if one exists. Note that these examples are illustrative, but that there are
11 sub-cases within many cases that do not affect the outcome (Fig. C1, Zeeman 1993). Our
12 Mathematica code can be used to generate additional results.
13
14

15 Competitive asymmetry
16
17 Our first five examples use the α -matrix used in Fig. 3C and Fig. 4, where $\bar{A} = 4$ and $\rho = 0.5$:

$$\alpha = \begin{bmatrix} 1 & 0.125 & 2 \\ 2 & 1 & 0.125 \\ 0.125 & 2 & 1 \end{bmatrix}$$

23 This results in the following outcome plot:
24
25
26
27
28
29
30
31
32
33
34
35
36
37
38
39
40
41
42
43
44
45
46
47
48
49
50
51
52
53
54



55
56
57
58
59 Figure A1. Outcome plot for first five numerical examples below.
60

i wins — $\{r_1, r_2, r_3\} = \{0.9, 0.05, 0.05\}$

Equilibrium	$\{\hat{N}_1, \hat{N}_2, \hat{N}_3\}$	Eigenvalues
{}	{0, 0, 0}	{0.9, 0.05, 0.05}
{1}	{0.9, 0, 0}	{-0.0625, -0.9, -1.75}
{2}	{0, 0.05, 0}	{0.89375, -0.05, -0.05}
{3}	{0, 0, 0.05}	{0.8, 0.04375, -0.05}
{1, 2}	{1.19167, -2.33333, 0}	Equilibrium not feasible
{1, 3}	{1.06667, 0, -0.0833333}	Equilibrium not feasible
{2, 3}	{0, 0.0583333, -0.066667}	Equilibrium not feasible
{1, 2, 3}	{0.0932544, -0.188402, 0.415148}	Equilibrium not feasible

The only equilibrium that is both feasible and stable is {1}.

i&j coexist — $\{r_1, r_2, r_3\} = \{0.2, 0.6, 0.2\}$

Equilibrium	$\{\hat{N}_1, \hat{N}_2, \hat{N}_3\}$	Eigenvalues
{}	{0, 0, 0}	{0.6, 0.2, 0.2}
{1}	{0.2, 0, 0}	{0.2, 0.175, -0.2}
{2}	{0, 0.6, 0}	{0.125, -0.6, -1}
{3}	{0, 0, 0.2}	{0.575, -0.2, -0.2}
{1, 2}	{0.166667, 0.266667, 0}	{-0.1, -0.333333, -0.354167}
{1, 3}	{-0.266667, 0, 0.233333}	Equilibrium not feasible
{2, 3}	{0, 0.766667, -1.33333}	Equilibrium not feasible
{1, 2, 3}	{0.251834, 0.100355, -0.0321893}	Equilibrium not feasible

The only equilibrium that is both feasible and stable is {1, 2}.

Heteroclinic cycle — $\{r_1, r_2, r_3\} = \{0.333333, 0.4, 0.266667\}$

Equilibrium	$\{\hat{N}_1, \hat{N}_2, \hat{N}_3\}$	Eigenvalues
{}	{0, 0, 0}	{0.4, 0.333333, 0.266667}
{1}	{0.333333, 0, 0}	{0.225, -0.266667, -0.333333}
{2}	{0, 0.4, 0}	{0.283333, -0.4, -0.533333}
{3}	{0, 0, 0.266667}	{0.366667, -0.266667, -0.2}
{1, 2}	{0.377777, -0.355555, 0}	Equilibrium not feasible
{1, 3}	{-0.266667, 0, 0.3}	Equilibrium not feasible
{2, 3}	{0, 0.488889, -0.711111}	Equilibrium not feasible
{1, 2, 3}	{0.154004, 0.0814204, 0.0845758}	{0.0036627 ± 0.163469i, -0.327325}

No equilibrium is both feasible and stable.

Invasion rates		Exclusion rates	
$\lambda_{1,2}$	0.283333	$\lambda_{2,1}$	-0.266667
$\lambda_{2,3}$	0.366667	$\lambda_{3,2}$	-0.533333
$\lambda_{3,1}$	0.225	$\lambda_{1,3}$	-0.2
$\lambda_{1,2}\lambda_{2,3}\lambda_{3,1}$	0.023375	$-\lambda_{2,1}\lambda_{3,2}\lambda_{1,3}$	0.0284445

The heteroclinic cycle {1} → {3} → {2} → {1} is stable since the product of exclusion rates is greater than the product of invasion rates. Dynamics are shown in Fig. 4a.

Limit cycle — $\{r_1, r_2, r_3\} = \{0.333333, 0.43, 0.236667\}$

Equilibrium	$\{\hat{N}_1, \hat{N}_2, \hat{N}_3\}$	Eigenvalues
{}	{0, 0, 0}	{0.43, 0.333333, 0.236667}
{1}	{0.333333, 0, 0}	{0.195, -0.236666, -0.333333}
{2}	{0, 0.43, 0}	{0.279583, -0.43, -0.623333}
{3}	{0, 0, 0.236667}	{0.400417, -0.14, -0.236667}
{1, 2}	{0.372777, -0.315555, 0}	Equilibrium not feasible
{1, 3}	{-0.186668, 0, 0.26}	Equilibrium not feasible
{2, 3}	{0, 0.533889, -0.831111}	Equilibrium not feasible
{1, 2, 3}	{0.175306, 0.0700594, 0.074635}	{0.000875562 ± 0.153325i, -0.321751}

No equilibrium is both feasible and stable.

Invasion rates		Exclusion rates	
$\lambda_{1,2}$	0.279583	$\lambda_{2,1}$	-0.236666
$\lambda_{2,3}$	0.400417	$\lambda_{3,2}$	-0.623333
$\lambda_{3,1}$	0.195	$\lambda_{1,3}$	-0.14
$\lambda_{1,2}\lambda_{2,3}\lambda_{3,1}$	0.0218302	$-\lambda_{2,1}\lambda_{3,2}\lambda_{1,3}$	0.0206532

The heteroclinic cycle $\{1\} \rightarrow \{3\} \rightarrow \{2\} \rightarrow \{1\}$ is unstable, since the product of invasion rates is greater than the product of exclusion rates. Therefore, there must be a stable limit cycle somewhere between unstable heteroclinic cycle and unstable three-species equilibrium.

Dynamics are shown in Fig. 4b.

1&2&3 coexist — $\{r_1, r_2, r_3\} = \{0.333333, 0.45, 0.216667\}$

Equilibrium	$\{\hat{N}_1, \hat{N}_2, \hat{N}_3\}$	Eigenvalues
{}	{0, 0, 0}	{0.45, 0.333333, 0.216667}
{1}	{0.333333, 0, 0}	{0.175, -0.216666, -0.333333}
{2}	{0, 0.45, 0}	{0.277083, -0.45, -0.683333}
{3}	{0, 0, 0.216667}	{0.422917, -0.1, -0.216667}
{1, 2}	{0.369444, -0.288888, 0}	Equilibrium not feasible
{1, 3}	{-0.133335, 0, 0.233334}	Equilibrium not feasible
{2, 3}	{0, 0.563889, -0.911111}	Equilibrium not feasible
{1, 2, 3}	{0.189507, 0.0624854, 0.0680078}	{-0.00126326 ± 0.144674i, -0.317473}

Only the three-species equilibrium {1, 2, 3} is both feasible and stable.

Invasion rates		Exclusion rates	
$\lambda_{1,2}$	0.277083	$\lambda_{2,1}$	-0.216666
$\lambda_{2,3}$	0.422917	$\lambda_{3,2}$	-0.683333
$\lambda_{3,1}$	0.175	$\lambda_{1,3}$	-0.1
$\lambda_{1,2}\lambda_{2,3}\lambda_{3,1}$	0.0205071	$-\lambda_{2,1}\lambda_{3,2}\lambda_{1,3}$	0.0148057

The heteroclinic cycle $\{1\} \rightarrow \{3\} \rightarrow \{2\} \rightarrow \{1\}$ is unstable, since the product of invasion rates is greater than the product of exclusion rates. Dynamics are shown in Fig. 4c.

1
2
3 Various founder control cases
4
56 The next three examples illustrate various cases of founder control, using the α -matrix from
7 Fig. S2 where $\rho_{12} = 2^{1/4}$, $\rho_{23} = 2^{1/4}$, $\rho_{31} = 2^{-1/4}$, and $A = 2^{1/4}$:

8
9
10
11
$$\alpha = \begin{bmatrix} 1 & 1 & 1 \\ 1.41421 & 1 & 1 \\ 0.707107 & 1.41421 & 1 \end{bmatrix}$$

12
13
14
15
16
17
18
19
20
21
22
23
24
25
26
27
28
29
30
31
32
33
34
35
36
37
38
39
40
41
42
43
44
45
46
47
48
49
50
51
52
53
54
55
56
57
58
59
60

This results in the following outcome plot:

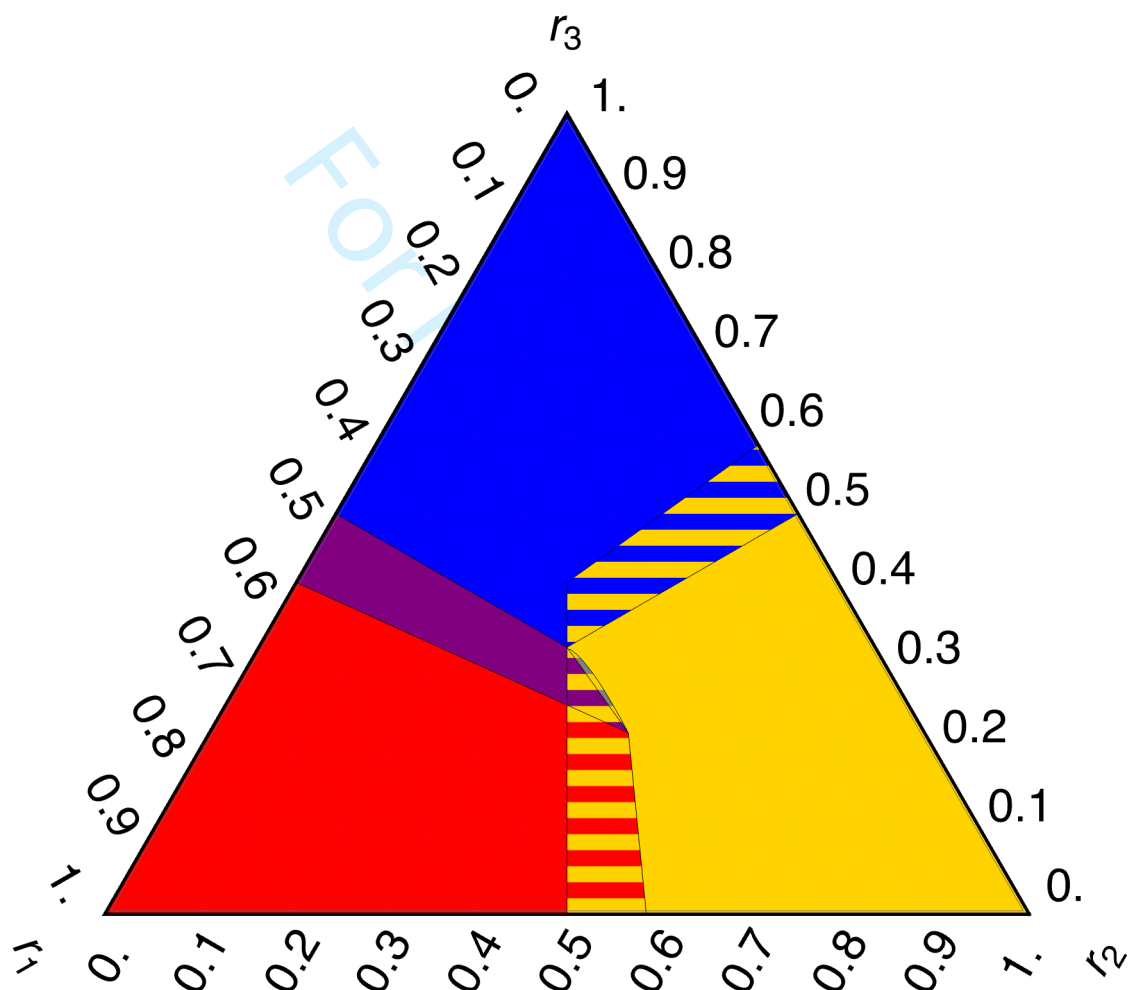


Figure A2. Outcome plot for next three numerical examples below.

i or j wins — $\{r_1, r_2, r_3\} = \{0.39, 0.45, 0.16\}$

Equilibrium	$\{\hat{N}_1, \hat{N}_2, \hat{N}_3\}$	Eigenvalues
{}	{0, 0, 0}	{0.45, 0.39, 0.16}
{1}	{0.39, 0, 0}	{-0.39, -0.115772, -0.101543}
{2}	{0, 0.45, 0}	{-0.476396, -0.45, -0.06}
{3}	{0, 0, 0.16}	{0.29, 0.23, -0.16}
{1, 2}	{0.144853, 0.245147, 0}	{-0.424638, -0.289117, 0.0346385}
{1, 3}	{0.785269, 0, -0.395269}	Equilibrium not feasible
{2, 3}	{0, -0.700122, 1.15012}	Equilibrium not feasible
{1, 2, 3}	{0.144853, -0.452843, 0.69799}	Equilibrium not feasible

Two equilibria are both feasible and stable: {1} and {2}.

i wins or j&k coexist — $\{r_1, r_2, r_3\} = \{0.35, 0.37, 0.28\}$

Equilibrium	$\{\hat{N}_1, \hat{N}_2, \hat{N}_3\}$	Eigenvalues
{}	{0, 0, 0}	{0.37, 0.35, 0.28}
{1}	{0.35, 0, 0}	{0.0325126, -0.124975, -0.35}
{2}	{0, 0.37, 0}	{-0.02, -0.243259, -0.37}
{3}	{0, 0, 0.28}	{0.09, 0.07, -0.28}
{1, 2}	{0.0482843, 0.301716, 0}	{0.0164662, -0.180833, -0.366466}
{1, 3}	{0.238995, 0, 0.111005}	{-0.0238225, -0.0789949, -0.326178}
{2, 3}	{0, -0.217279, 0.587279}	Equilibrium not feasible
{1, 2, 3}	{0.0482843, -0.134853, 0.436569}	Equilibrium not feasible

Two equilibria are both feasible and stable: {2} and {1, 3}.

i wins or 1&2&3 coexist — $\{r_1, r_2, r_3\} = \{0.323, 0.381, 0.296\}$

Equilibrium	$\{\hat{N}_1, \hat{N}_2, \hat{N}_3\}$	Eigenvalues
{}	{0, 0, 0}	{0.381, 0.323, 0.296}
{1}	{0.323, 0, 0}	{0.0676045, -0.075791, -0.323}
{2}	{0, 0.381, 0}	{-0.058, -0.242815, -0.381}
{3}	{0, 0, 0.296}	{0.085, 0.027, -0.296}
{1, 2}	{0.140024, 0.182976, 0}	{0.030059, -0.0617788, -0.353059}
{1, 3}	{0.0921838, 0, 0.230816}	{0.0198162, -0.0206092, -0.302391}
{2, 3}	{0, -0.205208, 0.586208}	Equilibrium not feasible
{1, 2, 3}	{0.140024, 0.0338284, 0.149147}	{-0.00264933 ± 0.0193523i, -0.317701}

Two equilibria are both feasible and stable: {2} and {1, 2, 3}.

Remaining examples

The remaining examples each use different α -matrices, so we don't present the corresponding outcome plots.

i&j coexist or i&k coexist

Here we use the α -matrix from Fig. S2 with $\rho_{12} = 2^{-3/4}$, $\rho_{23} = 2^{-3/4}$, $\rho_{31} = 2^{3/4}$, and $A = 1$:

$$\alpha = \begin{bmatrix} 1 & 0.594604 & 1.68179 \\ 0.594604 & 1 & 0.594604 \\ 1.68179 & 0.594604 & 1 \end{bmatrix}$$

and growth rates $\{r_1, r_2, r_3\} = \{0.333333, 0.333333, 0.333333\}$.

Equilibrium	$\{\hat{N}_1, \hat{N}_2, \hat{N}_3\}$	Eigenvalues
{}	{0, 0, 0}	{0.333333, 0.333333, 0.333333}
{1}	{0.333333, 0, 0}	{0.135132, -0.227264, -0.333333}
{2}	{0, 0.333333, 0}	{0.135132, -0.227264, -0.333333}
{3}	{0, 0, 0.333333}	{0.135132, -0.227264, -0.333333}
{1, 2}	{0.209038, 0.209038, 0}	{-0.0847433, -0.14252, -0.333333}
{1, 3}	{0.124295, 0, 0.124295}	{0.185521, 0.0847434, -0.333333}
{2, 3}	{0, 0.209038, 0.209038}	{-0.0847433, -0.14252, -0.333333}
{1, 2, 3}	{0.0684324, 0.251953, 0.068432}	{0.0466566, -0.102141, -0.333333}

Two equilibria are both feasible and stable: {1, 2} and {2, 3}.

1 or 2 or 3 wins

Here we use the α -matrix from Fig. 2H with $\rho = 2$ and $A = 1$:

$$\alpha = \begin{bmatrix} 1 & 2 & 2 \\ 2 & 1 & 2 \\ 2 & 2 & 1 \end{bmatrix}$$

and growth rates $\{r_1, r_2, r_3\} = \{0.333333, 0.333333, 0.333333\}$.

Equilibrium	$\{\hat{N}_1, \hat{N}_2, \hat{N}_3\}$	Eigenvalues
{}	{0, 0, 0}	{0.333333, 0.333333, 0.333333}
{1}	{0.333333, 0, 0}	{-0.333333, -0.333333, -0.333333}
{2}	{0, 0.333333, 0}	{-0.333333, -0.333333, -0.333333}
{3}	{0, 0, 0.333333}	{-0.333333, -0.333333, -0.333333}
{1, 2}	{0.111111, 0.111111, 0}	{0.111111, -0.111111, -0.333333}
{1, 3}	{0.111111, 0, 0.111111}	{0.111111, -0.111111, -0.333333}
{2, 3}	{0, 0.111111, 0.111111}	{0.111111, -0.111111, -0.333333}
{1, 2, 3}	{0.0666667, 0.0666667, 0.0666667}	{0.0666667, 0.0666667, -0.333333}

Three equilibria are both feasible and stable: {1}, {2}, and {3}.

1
2
3 1&2&3 coexist or heteroclinic cycle
4

5 Here we use the α -matrix from Fig. S4a-d with $\rho = 0.5$, $A_{12} = 32$, $A_{23} = 4$, and $A_{31} = 0.5$:
6

$$\alpha = \begin{bmatrix} 1 & 0.015625 & 0.25 \\ 16 & 1 & 0.125 \\ 1 & 2 & 1 \end{bmatrix}$$

7
8
9
10
11 and growth rates $\{r_1, r_2, r_3\} = \{0.0833333, 0.666667, 0.666667\}$.
12
13

Equilibrium	$\{\hat{N}_1, \hat{N}_2, \hat{N}_3\}$	Eigenvalues
{}	{0, 0, 0}	{0.666667, 0.666667, 0.0833333}
{1}	{0.0833333, 0, 0}	{0.583333, -0.0833333, -0.666667}
{2}	{0, 0.666667, 0}	{0.0729167, -0.666667, -0.666667}
{3}	{0, 0, 0.666667}	{0.583333, -0.0833333, -0.666667}
{1, 2}	{0.0972222, -0.888889, 0}	Equilibrium not feasible
{1, 3}	{-0.111111, 0, 0.777778}	Equilibrium not feasible
{2, 3}	{0, 0.777778, -0.888889}	Equilibrium not feasible
{1, 2, 3}	{0.0266667, 0.213333, 0.213333}	{-0.0222235 ± 0.154916i, -0.408886}

26 Only the three-species equilibrium {1, 2, 3} is both feasible and stable. We investigate the
27 existence of a heteroclinic cycle below by calculating invasion (exclusion) rates into (from)
28 monocultures.
29

Invasion rates		Exclusion rates	
$\lambda_{1,2}$	0.0729167	$\lambda_{2,1}$	-0.666667
$\lambda_{2,3}$	0.583333	$\lambda_{3,2}$	-0.666667
$\lambda_{3,1}$	0.583333	$\lambda_{1,3}$	-0.0833333
$\lambda_{1,2}\lambda_{2,3}\lambda_{3,1}$	0.0248119	$-\lambda_{2,1}\lambda_{3,2}\lambda_{1,3}$	0.037037

30 Since $\lambda_{1,2} > 0 > \lambda_{2,1}$, $\lambda_{2,3} > 0 > \lambda_{3,2}$ and $\lambda_{3,1} > 0 > \lambda_{1,3}$, the heteroclinic cycle $\{1\} \rightarrow$
31 $\{3\} \rightarrow \{2\} \rightarrow \{1\}$ exists. Due to the positive signs of $\lambda_{1,2}$, $\lambda_{2,3}$, $\lambda_{3,1}$ and the negative signs of
32 $\lambda_{2,1}$, $\lambda_{3,2}$, $\lambda_{1,3}$, we label these invasion rates and exclusion rates respectively in the table
33 above. The heteroclinic cycle $\{1\} \rightarrow \{3\} \rightarrow \{2\} \rightarrow \{1\}$ is also stable since the product of
34 exclusion rates is greater than the product of invasion rates.
35

36 Dynamics of the two attractors are shown in Fig. S5ab.
37

38
39
40
41
42
43
44
45
46
47
48
49
50
51
52
53
54
55
56
57
58
59
60

Appendix B: Constructing and reading a feasibility plot

Saavedra et al. (2017) focused on the unit simplex $r_1 + r_2 + r_3 = 1$ (Fig. B1) to visualize and analyze the feasibility and structural stability of multi-species equilibria. Using the unit simplex reduces the dimensionality of the parameter space, simplifying its exploration, while having no practical consequences since structural properties are invariant under multiplying all r_i 's by a constant. In practice, any set of r_i 's can be analyzed on the unit simplex after rescaling the r_i 's by their sum $r_1 + r_2 + r_3$.

Within the simplex, each point represents a collection of r_i such that $r_1 + r_2 + r_3 = 1$. Moving around in the simplex changes the r_i values of each species while the total still sums to one. In particular, each of the three vertices of the triangle correspond to a single species i , since there we have $r_i = 1$ and the other two r_j 's being zero and thus excluded (Fig. B1). Each edge of the triangle corresponds to a given pair of species corresponding to the vertices of the edge, with the third species excluded. For example, points on the bottom edge of the triangle in Fig. B1 correspond to the pair of species 1 and 2 with species 3 absent. The centroid of the triangle corresponds to $\{r_1, r_2, r_3\} = \{1/3, 1/3, 1/3\}$ and represents a situation where the intrinsic growth rate of all three species is equal. Moving from the centroid towards a vertex ($r_i = 1$) results in an increase in r_i with a corresponding decrease in the other two r_j values.

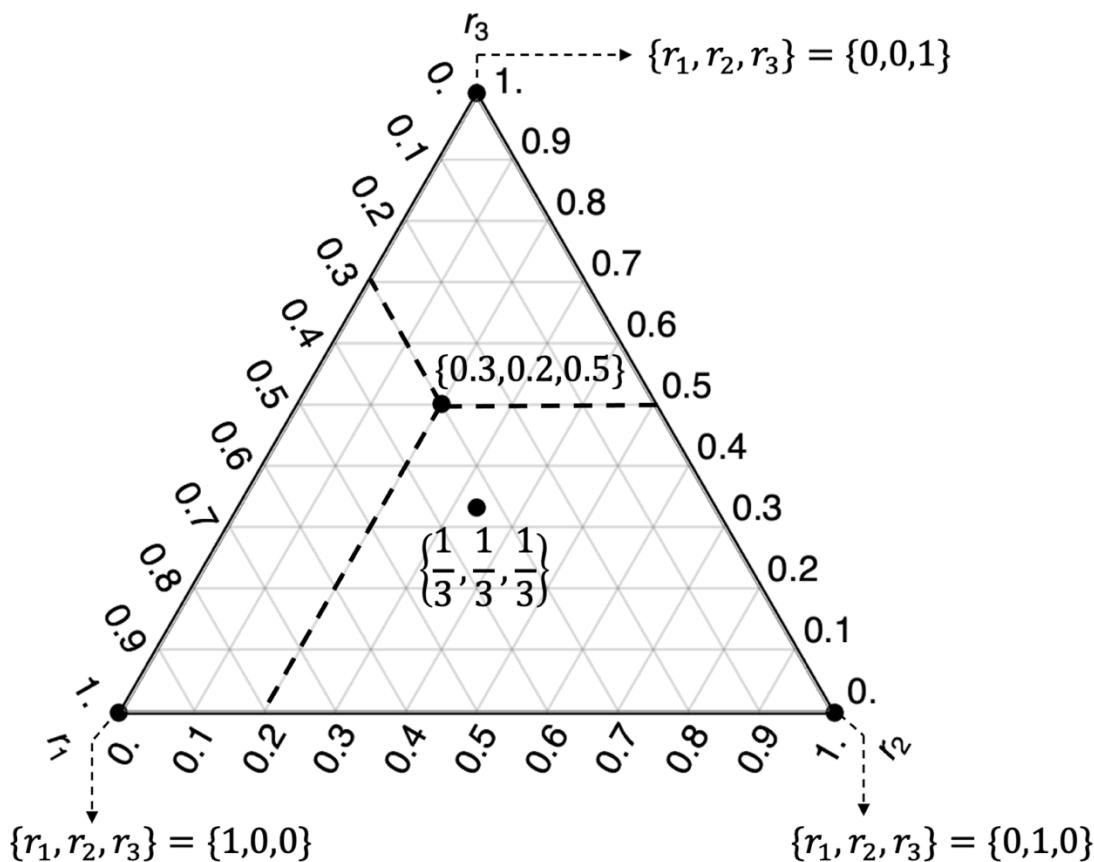


Figure B1. The intrinsic growth rate ($r_1 - r_2 - r_3$) unit simplex. At the vertices, one species' intrinsic growth rate ($r_i = 1$) and $r_j = 0$ for the other two species. At the centroid of the triangle, $\{r_1, r_2, r_3\} = \{1/3, 1/3, 1/3\}$ and the intrinsic growth rates of all species are equal.

The r_i values of any point on the simplex can be read using the grid in the background (grey grid in Fig. B1). The grid lines run parallel to the three simplex edges and are equally spaced. At any edge $r_i - r_j$, $r_k = 0$. As we move further from the $r_i - r_j$ edge ($r_k = 0$) towards the opposite vertex ($r_k = 1$), r_k is constant on each grid line parallel to the $r_i - r_j$ edge and increases as we approach the vertex $r_k = 1$. Every point on the simplex lies at the intersection of three such grid lines – one parallel to each edge. Therefore, the r values of any point can simply be read by finding the three grid lines that intersect at that point and finding the r value constant on each of those edges.

As an example, we use the point $\{r_1, r_2, r_3\} = \{0.3, 0.2, 0.5\}$ marked in Fig. B1. The dashed lines in black represent the three grid lines that meet at the focal point. The r_1 value can be read from the grid lines parallel to the $r_2 - r_3$ edge. As can be seen in the figure, the grid line parallel to the $r_2 - r_3$ edge passing through our focal point represents $r_1 = 0.3$. The r_2 value can be read from the grid lines parallel to the $r_1 - r_3$ edge. For the point in this example, the grid line parallel to the $r_1 - r_3$ edge represents $r_2 = 0.2$. Finally, the r_3 value can be read from the horizontal grid lines parallel to the $r_1 - r_2$ edge. For our example, the grid line parallel to the $r_1 - r_2$ edge represents $r_3 = 0.5$.

Following the structural stability framework, the range of r_i values for which the various equilibria are feasible can be calculated and shown graphically on the $r_1 - r_2 - r_3$ simplex (Saavedra et al. 2017). In a three-species LV model, there are three one-species equilibria (the ‘monocultures’), three two-species equilibria (the ‘pairs’) and one three-species equilibrium (the ‘triplet’). The one-species equilibria are always feasible, covering the whole unit simplex. Therefore, we omit showing them on the simplex. The boundaries of feasibility regions of pairwise equilibrium $\{i, j\}$ can be calculated by setting the equilibrium densities of species i and j (Table A1) equal to zero and solving them for r_i and r_j on the edge $r_i + r_j = 1$:

$$\widehat{N}_i = \frac{r_i \alpha_{jj} - r_j \alpha_{ij}}{\alpha_{ii} \alpha_{jj} - \alpha_{ij} \alpha_{ji}} = 0, \widehat{N}_j = \frac{r_j \alpha_{ii} - r_i \alpha_{ji}}{\alpha_{ii} \alpha_{jj} - \alpha_{ij} \alpha_{ji}} = 0, r_i + r_j = 1$$

When combined with the opposite vertex ($r_k = 1$), the feasibility region for the pairwise equilibrium $\{i, j\}$ within the unit simplex is triangular with the vertices:

$$(r_i, r_j, r_k) = \left(\frac{\alpha_{ij}}{\alpha_{ij} + \alpha_{jj}}, \frac{\alpha_{jj}}{\alpha_{ij} + \alpha_{jj}}, 0 \right), \left(\frac{\alpha_{ji}}{\alpha_{ji} + \alpha_{ii}}, \frac{\alpha_{ii}}{\alpha_{ji} + \alpha_{ii}}, 0 \right), (0, 0, 1)$$

Within the structural stability framework, larger feasibility regions correspond to more structurally stable equilibria since a small change in the r_i values due to changing environments is unlikely to make the equilibrium infeasible. But this completely ignores the dynamical stability of these equilibria even though feasible, dynamically unstable equilibria are not states where an ecological system would spend much time. To fill this gap, we calculate the stability of the pairwise equilibria $\{i, j\}$ within its feasibility region using mutual invasibility criteria (Table A1):

$$\lambda_{i,j} > 0 \text{ & } \lambda_{j,i} > 0$$

We calculate the stability of the pairwise equilibria over its feasibility region numerically, assuming that the third species is absent. Note that the stability of pairwise equilibria in the unit simplex can also be calculated analytically, however numerical methods become necessary for calculating the stability of the three-species equilibrium. Considering a pair in isolation, the stability of its equilibrium does not change within its feasibility region in the unit simplex. If a pairwise equilibrium is stable (unstable) at one point within the feasibility region, it is stable (unstable) throughout the feasibility region. Therefore, for pairwise equilibria, the feasibility and stability regions are identical.

It is important to recognize that the feasibility and stability regions are identical only for pairwise equilibria in *isolation*. When the third species is considered, the pairwise equilibrium can potentially be invaded by the third species in part of the feasibility region. Therefore, the feasibility and stability regions of a pairwise equilibrium are not always identical when the third species in the triplet is considered. Further, the stability of a three-species equilibrium can change within the feasibility region. Despite these limitations, calculating the stability regions of pairwise equilibria in isolation is helpful to understand the dynamics of the triplet as can be seen below and in the main text.

To calculate the boundaries of the feasibility region of the three-species equilibrium, we set the densities of the three species equal to zero and project it on the unit simplex:

$$\widehat{\vec{N}} = \alpha^{-1} \vec{r} = 0 \quad \& \quad r_1 + r_2 + r_3 = 1$$

To demonstrate the construction of a feasibility plot in more detail, we use Fig. 2A in the main text as an example (Fig. B2). We show stable pairwise equilibria in the unit simplex in orange and unstable pairwise equilibria in lavender (Figs. 2, 3 in main text, Figs. B2, B3 in Appendix B). Fig. 2a considers a symmetric case where the pairwise niche differences are such that each pairwise equilibrium is stable. We first calculate the region in the unit simplex where the pairwise equilibrium of species 1 and 2 is feasible and stable (orange vertical triangle in Fig. B2a). Note that the triangular feasibility region for the species 1 & 2 pair is grounded on the $r_1 - r_2$ edge. In the next two steps, we overlay the feasibility region of species 2 & 3 (Fig. B2b) and species 1 & 3 (Fig. B2c) on the unit simplex. Finally, we overlay the feasibility region of the three-species equilibrium (gray triangle in Fig. B2d) on the unit simplex, completing the feasibility plot.

Next, we explore the final feasibility plot from Fig. B2d (and Fig. 2a in the main text) in detail to build some intuition about reading feasibility plots (Fig. B3). The complete feasibility plot is shown in Fig. B3a. The regions in white denote values of r_i where no pairwise equilibrium is feasible (Fig. B3b). The feasibility regions of the three pairwise equilibria overlap in a variety of ways, resulting in regions consisting of one (Fig. B3c), two (Fig. B3d) or three (Fig. B3e) feasible pairwise equilibria. Finally, the gray region in the center shows a case where all three pairwise equilibria and the three-species equilibrium are feasible (Fig. B3f).

The reader should note that the feasibility plot shown here has been chosen to be especially symmetric for pedagogical purposes — all three pairwise equilibria $\{i, j\}$ are stable and their feasibility regions intersect the $r_i - r_j$ edge at $\{r_i = 1/3, r_j = 2/3, r_k = 0\}$ and $\{r_i = 2/3, r_j = 1/3, r_k = 0\}$, thus occupying the center one-third of the edge. The pairwise

1
2
3
4
5
6
7
8
9
10
11
12
13
14
15
16
17
18
19
20
21
22
23
24
25
26
27
28
29
30
31
32
33
34
35
36
37
38
39
40
41
42
43
44
45
46
47
48
49
50
51
52
53
54
55
56
57
58
59
60

feasibility regions also intersect in the center of the unit simplex and the three-species feasibility region is centered on the centroid of the unit simplex. These symmetrical features are by no means universal and we explore some of the ways in which the symmetries can be broken and their impact on the feasibility regions in Figs. 2, 3, 5, S2-4.

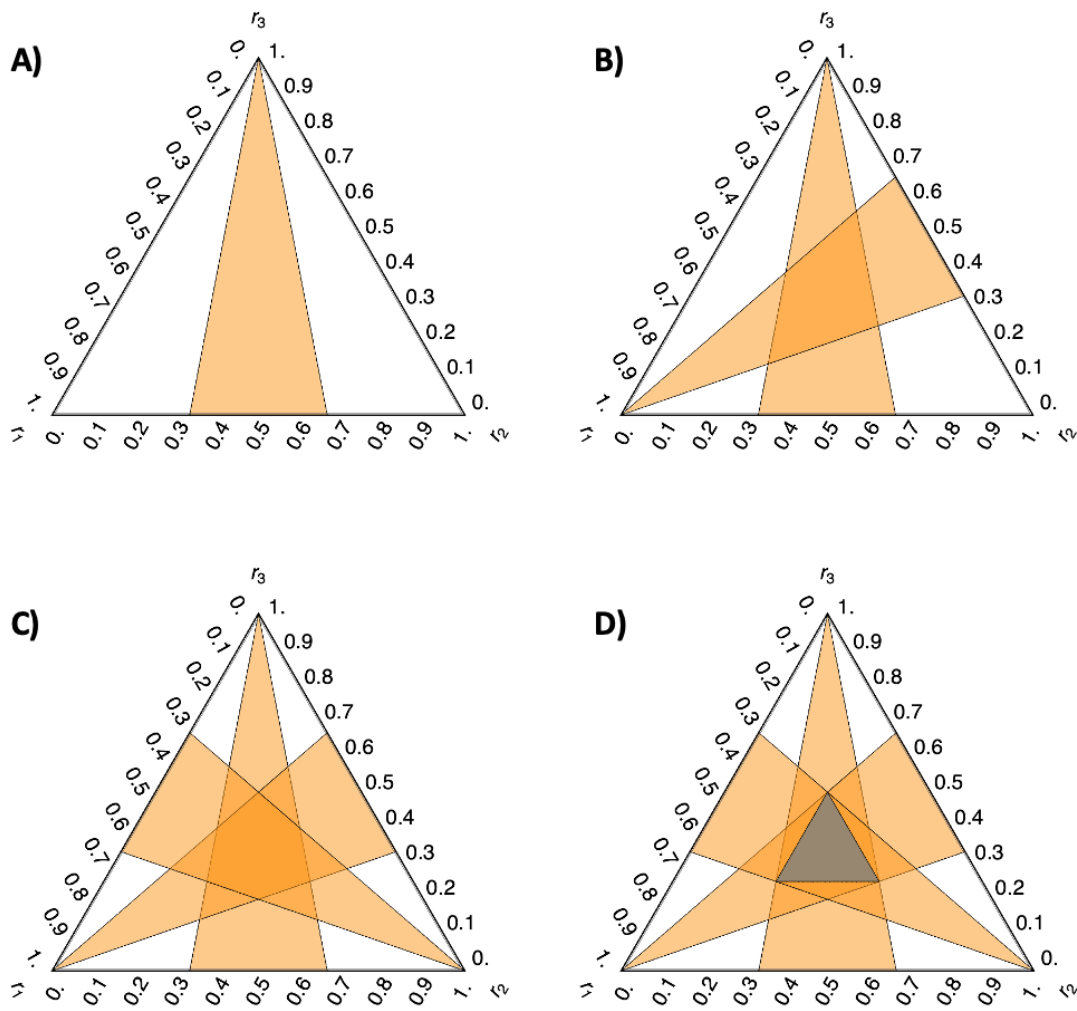


Figure B2. Building a feasibility plot. We show a stepwise construction of the feasibility plot in Fig. 2a in the main text, where all pairwise equilibria are stable. The orange filling of the triangles represents a stable pairwise equilibrium, whereas a lavender filling represents an unstable pairwise equilibrium (not encountered here, but present in Fig. 2a). For pairwise equilibria, feasibility and stability regions are identical. So, we refer to them just as feasibility regions here. **(a)** The vertical orange triangle (vertex on $\{r_1, r_2, r_3\} = \{0, 0, 1\}$) in the unit simplex shows the region where the pairwise equilibrium for species 1&2 is feasible. **(b)** The left orange triangle (vertex on $\{r_1, r_2, r_3\} = \{1, 0, 0\}$) overlaid on Fig. B2a represents the feasibility region for the pairwise equilibrium of species 2&3. **(c)** The right orange triangle (vertex on $\{r_1, r_2, r_3\} = \{0, 1, 0\}$) overlaid on Fig. B2b represents the feasibility region of the third and final pair of species 1&3. **(d)** The dark gray triangle in the center overlaid on Fig. B2c shows the feasibility region of the three-species equilibrium and completes the feasibility plot.

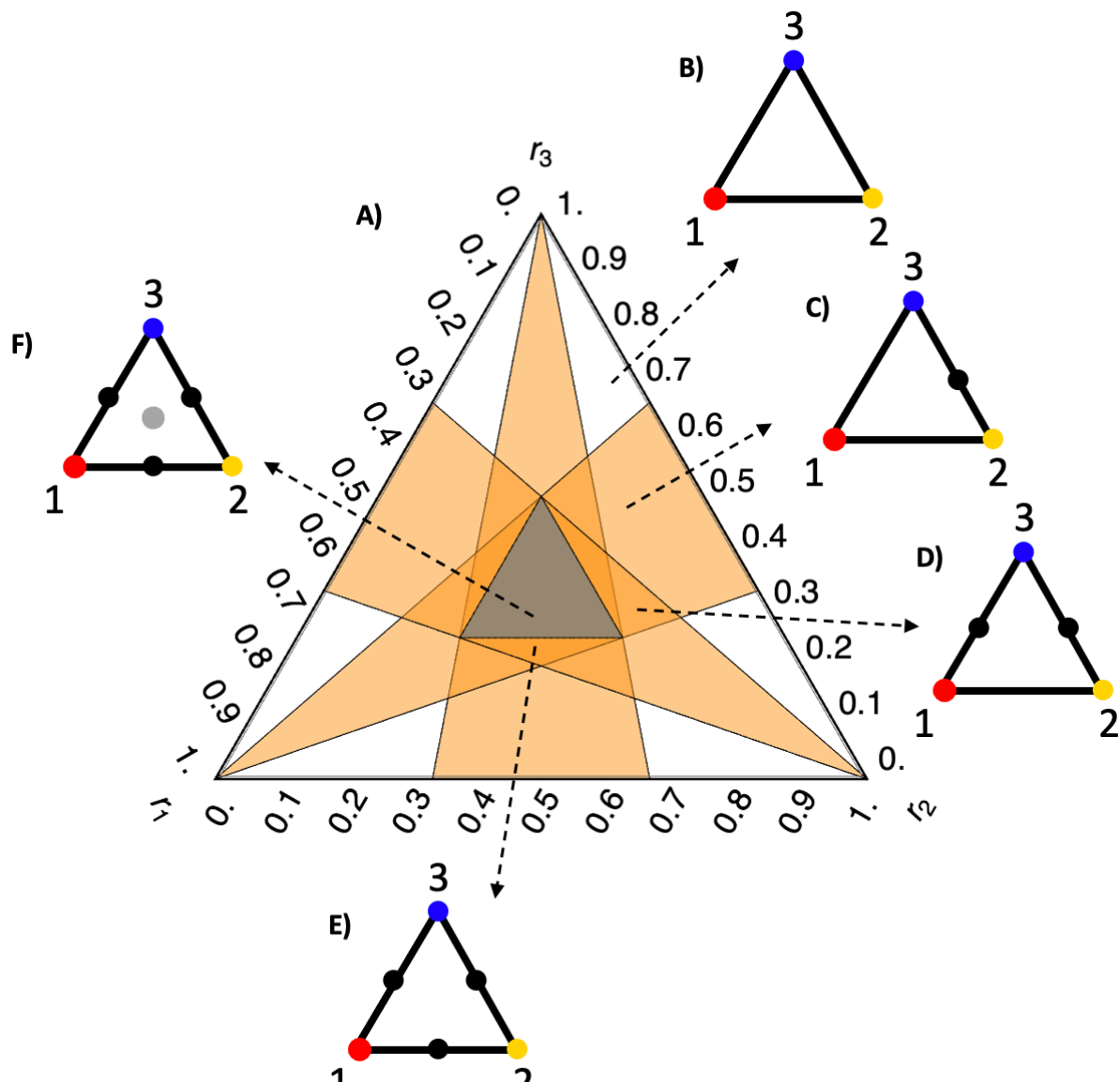


Figure B3. Exploration of a feasibility plot. Here, we explore various regions of the feasibility plot — shown in **(a)** here — we built in Fig. B2. For each region, we draw a phase portrait of the system where we show the 2 species and 3 species equilibria as filled black circles if stable, open circles if unstable (not encountered here) and filled gray circles if stability is unknown. **(b)** In the white regions, the values of r_i are such that there are no feasible pairwise equilibria as can be seen from the lack of edge circles in the phase portrait. **(c)** In the regions with only one orange pairwise feasibility region, only one pairwise equilibrium is stable. In this case, the feasibility region intersects the edge of the pair 2&3. Therefore, the pairwise equilibrium of species 2&3 is stable, as can be seen by the black dot on the 2&3 edge in the phase portrait. **(d)** In the regions with two overlapping orange pairwise feasibility regions, two pairwise equilibria (1&3 and 2&3) are stable. **(e)** In the regions with three overlapping orange pairwise feasibility regions, all three pairwise equilibria (1&3, 2&3 and 1&2) are stable. **(f)** Finally, in the region with three orange pairwise feasibility regions and a gray three-species equilibrium feasibility region, all three pairwise equilibria (1&3, 2&3 and 1&2) are stable and the three-species equilibrium is feasible (gray circle in the center of the phase portrait).

Appendix C: Reading feasibility and outcome plots together

While feasibility plots show us feasibility regions of all equilibria and stability regions of pairwise equilibria on the unit simplex, they don't show us the dynamical outcome of competition. Since competition outcomes are of interest, we construct *outcome plots* to help us understand the dynamical outcome as the intrinsic growth rate (r_i) changes. The construction process of these plots is detailed in Appendix A. Here, we compare a feasibility plot to the corresponding outcome plot to explain how they relate to each other.

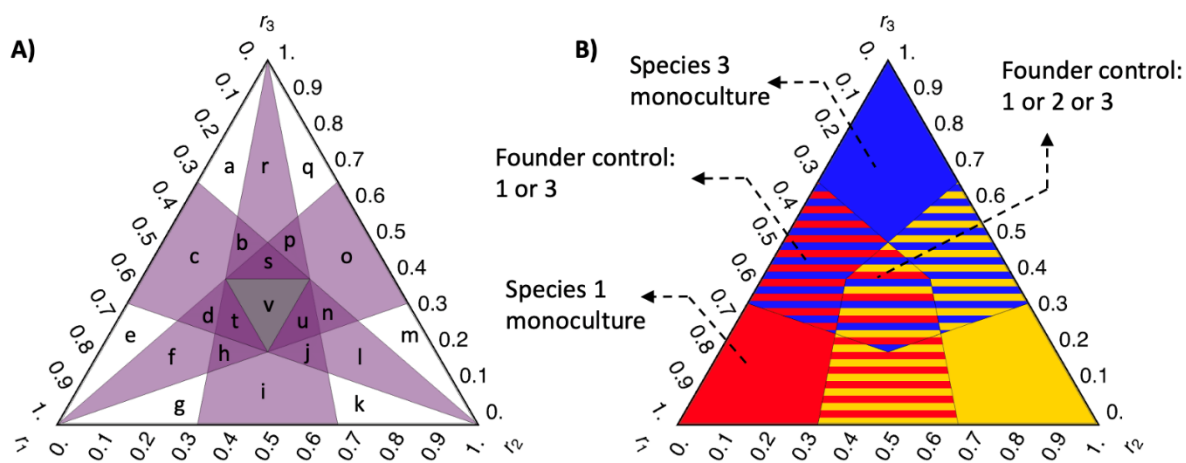


Figure C1. Reading a (a) feasibility and (b) outcome plot together. We show the plots from Figs. 2g and h here to explain their correspondence. In this case, all three pairwise equilibria are unstable as seen by the lavender color in Fig. C1a. Regions with different feasibility and stability configurations of equilibria are marked with different letters (regions a-v) in Fig. C1a. Regions a, r and q correspond to the blue-colored region in Fig. C1b, resulting in a species 3 monoculture. Similarly, regions e, f and g result in a species 1 monoculture (red-colored region in Fig. C1b). Regions b, c and d result in founder control between species 1 and 3 (red and blue stripes in Fig. C1b). Finally, the regions s,t,u and v in the center all result in a three-way founder control between the monocultures of species 1 or 2 or 3 (red, yellow and blue stripes in Fig. C1b).

We use Figs. 2g and 2h as a case study to explain how the feasibility plot and outcome plot relate to each other. In Fig. C1, the feasibility plot is shown on the left (Fig. C1a, also Fig. 2g in the main text) and the corresponding outcome plot is shown on the right (Fig. C1b, also Fig. 2h in the main text). The three pairwise equilibria are all unstable in this case, which can be seen by the lavender color of their feasibility regions in Fig. C1a. All possible intersections of the three pairwise feasibility regions create a plethora of parameter regions in Fig. C1a with different configurations of stability for pairwise equilibria and feasibility for the three-species equilibrium. Here, we mark each such region with a letter to facilitate comparison with the outcome plot. For a detailed guide on how to infer the equilibria and their feasibility status from a feasibility plot, refer to Appendix B.

Comparing the same region in the unit simplex between the feasibility and outcome plots highlights the differences between structural stability and competitive outcome. Near the r_3 vertex in Fig. C1a, regions a and q don't have any feasible pairwise or three-species equilibrium while the pairwise equilibrium $\{1,2\}$ is feasible and unstable in region r. However, all three of these regions (a, q and r in Fig. C1a) result in the same competitive outcome: a monoculture of species 3 (blue region at the top in Fig. C1b).

Moving downwards along the $r_1 - r_3$ edge, the region c has one unstable pairwise equilibrium $\{1,3\}$ while the regions b $\{1,3\}, \{1,2\}$ and d $\{1,3\}, \{2,3\}$ have two unstable pairwise equilibria. All three of these regions (b, c and d) result in founder control between species 1 and 3 (red and blue stripes in Fig. C1b). Due to the symmetric parameters for this figure, regions h, i, j and n, o, p show a similar pattern: the competitive outcome is founder control between two monocultures while the feasibility of pairwise equilibria varies. The symmetric parameters also result in the same relationship between feasibility and competitive outcome near the r_1 vertex and r_2 vertex as the one near the r_3 vertex. Near the r_1 vertex, regions e and g don't have any feasible pairwise or three-species equilibria while the pairwise equilibrium $\{2,3\}$ is feasible but unstable in region f. All three regions (e, f and g) result in a monoculture of species 1.

In the center of Fig. C1a, the regions s, t and u each have three feasible and unstable pairwise equilibria but no three-species equilibrium. In contrast, the central gray region v has all three feasible and unstable pairwise equilibria in addition to a feasible three-species equilibrium. Interestingly, all four regions (s, t, u and v) result in a three-way founder control between monocultures of species 1, 2 and 3 (red, yellow and blue stripes in the center of Fig. C1b).

Reading the feasibility and outcome plots together highlights the complex relationship between feasibility of equilibria and the dynamical outcomes. The rest of the rows in Fig. 2 in the main text compare the feasibility and outcome plots for the cases when there are zero (Figs. 2ab), one (Figs. 2cd) or two (Figs. 2ef) unstable pairwise equilibria. The rows in Fig. 3 in the main text do a similar comparison as the intransitivity of the triplet is increased. As explained here, the feasibility and outcome plots within these rows should be read together and compared to each other to maximize understanding.

Appendix D: Nondimensionalization

Here we show that the number of parameters in the three-species Lotka-Volterra competition model can be reduced from twelve to eight through nondimensionalization. The original, dimensional model is given by Eqn. (1) with $\mathcal{N} = 3$:

$$\frac{dN_1}{dt} = (r_1 - \alpha_{11}N_1 - \alpha_{12}N_2 - \alpha_{13}N_3)N_1 \quad (\text{D1a})$$

$$\frac{dN_2}{dt} = (r_2 - \alpha_{21}N_1 - \alpha_{22}N_2 - \alpha_{23}N_3)N_2 \quad (\text{D1b})$$

$$\frac{dN_3}{dt} = (r_3 - \alpha_{31}N_1 - \alpha_{32}N_2 - \alpha_{33}N_3)N_3 \quad (\text{D1c})$$

We rescale time by the sum of the intrinsic growth rates by letting $t^* = (r_1 + r_2 + r_3)t$, and population densities by letting $N_i^* = (\alpha_{ii}/(r_1 + r_2 + r_3))N_i$:

$$\frac{dN_1^*}{dt^*} = (r_1^* - N_1^* - \alpha_{12}^*N_2^* - \alpha_{13}^*N_3^*)N_1^* \quad (\text{D2a})$$

$$\frac{dN_2^*}{dt^*} = (r_2^* - \alpha_{21}^*N_1^* - N_2^* - \alpha_{23}^*N_3^*)N_2^* \quad (\text{D2b})$$

$$\frac{dN_3^*}{dt^*} = (r_3^* - \alpha_{31}^*N_1^* - \alpha_{32}^*N_2^* - N_3^*)N_3^* \quad (\text{D2c})$$

where $r_i^* = r_i/(r_1 + r_2 + r_3)$ and $\alpha_{ij}^* = \alpha_{ij}/\alpha_{jj}$. Note that $r_1^* + r_2^* + r_3^* = 1$, as assumed without loss of generality in the main text, so that there are only two independent r_i^* plus six interspecific competition coefficients α_{ij}^* — eight effective parameters.

A similar procedure results in the reduction of the free parameters in a two-species LV competition model from six to three. The original two-species model ($\mathcal{N} = 2$) is:

$$\frac{dN_1}{dt} = (r_1 - \alpha_{11}N_1 - \alpha_{12}N_2)N_1 \quad (\text{D3a})$$

$$\frac{dN_2}{dt} = (r_2 - \alpha_{21}N_1 - \alpha_{22}N_2)N_2 \quad (\text{D3b})$$

As before, we rescale time by the sum of the intrinsic growth rates by letting $t^* = (r_1 + r_2)t$, and population densities by letting $N_i^* = (\alpha_{ii}/(r_1 + r_2))N_i$:

$$\frac{dN_1^*}{dt^*} = (r_1^* - N_1^* - \alpha_{12}^*N_2^*)N_1^* \quad (\text{D4a})$$

$$\frac{dN_2^*}{dt^*} = (r_2^* - \alpha_{21}^*N_1^* - N_2^*)N_2^* \quad (\text{D4b})$$

1
2
3 Here, $r_i^* = r_i/(r_1 + r_2)$ and $\alpha_{ij}^* = \alpha_{ij}/\alpha_{jj}$. On the unit simplex for two species, $r_1^* + r_2^* = 1$,
4 so that there is only one independent r_i^* plus two interspecific competition coefficients α_{ij}^*
5 — resulting in a total of three effective parameters.
6
7
8
9
10
11
12
13
14
15
16
17
18
19
20
21
22
23
24
25
26
27
28
29
30
31
32
33
34
35
36
37
38
39
40
41
42
43
44
45
46
47
48
49
50
51
52
53
54
55
56
57
58
59
60

For Review Only

1
2
3 Appendix E: Parameter values for figures
4
5

6 Fig. 2ab:

7
8
9
10
$$\alpha = \begin{bmatrix} 1 & 0.5 & 0.5 \\ 0.5 & 1 & 0.5 \\ 0.5 & 0.5 & 1 \end{bmatrix}$$

11

12 Fig. 2cd:

13
14
15
16
$$\alpha = \begin{bmatrix} 1 & 2 & 0.5 \\ 2 & 1 & 0.5 \\ 0.5 & 0.5 & 1 \end{bmatrix}$$

17
18

19 Fig. 2ef:

20
21
22
23
$$\alpha = \begin{bmatrix} 1 & 0.5 & 2 \\ 0.5 & 1 & 2 \\ 2 & 2 & 1 \end{bmatrix}$$

24
25

26 Fig. 2gh:

27
28
29
30
$$\alpha = \begin{bmatrix} 1 & 2 & 2 \\ 2 & 1 & 2 \\ 2 & 2 & 1 \end{bmatrix}$$

31
32

33 Fig. 3ab:

34
35
36
37
$$\alpha = \begin{bmatrix} 1 & 0.5 & 0.5 \\ 0.5 & 1 & 0.5 \\ 0.5 & 0.5 & 1 \end{bmatrix}$$

38
39

40 Fig. 3cd:

41
42
43
44
$$\alpha = \begin{bmatrix} 1 & 0.166667 & 1.5 \\ 1.5 & 1 & 0.166667 \\ 0.166667 & 1.5 & 1 \end{bmatrix}$$

45
46

47 Fig. 3ef:

48
49
50
51
$$\alpha = \begin{bmatrix} 1 & 0.125 & 2 \\ 2 & 1 & 0.125 \\ 0.125 & 2 & 1 \end{bmatrix}$$

52
53

54 Fig. 4:

55
56
57
58
$$\alpha = \begin{bmatrix} 1 & 0.125 & 2 \\ 2 & 1 & 0.125 \\ 0.125 & 2 & 1 \end{bmatrix}$$

59
60

1
2
3 Fig. 4a:
4
5 $\vec{r} = [0.333333, 0.4, 0.266667]$
6
7
8 Fig. 4b:
9
10 $\vec{r} = [0.333333, 0.43, 0.236667]$
11
12 Fig. 4c:
13
14 $\vec{r} = [0.333333, 0.45, 0.216667]$
15
16
17
18
19
20
21
22
23
24
25
26
27
28
29
30
31
32
33
34
35
36
37
38
39
40
41
42
43
44
45
46
47
48
49
50
51
52
53
54
55
56
57
58
59
60

For Review Only

Appendix F — Inverse competition matrix exploration

Because the expression for the three-species equilibrium is

$$\hat{\vec{N}} = \alpha^{-1} \vec{r}$$

(Table A1), the inverse competition matrix, α^{-1} , gives the total effect (direct plus indirect effects) of a change in the intrinsic growth rates \vec{r} on the equilibrium densities $\hat{\vec{N}}$ (Bender et al. 1984). In this appendix, we point out some interesting connections between the inverse competition matrix and the structure of feasibility and outcome plots.

In the following examples, $\rho_{12} = \rho_{23} = \rho_{31} = \rho = 0.5$, as in Fig. 3, and we increase cyclic asymmetry $A_{12} = A_{23} = A_{31} = \bar{A}$.

When there is no cyclic asymmetry ($\bar{A} = 1$), the three-species coexistence feasibility region is inscribed in the intersection of the three pairwise-feasibility regions (Fig. F1). In this case, the inverse competition matrix is

$$\alpha^{-1} = \begin{bmatrix} 1.5 & -0.5 & -0.5 \\ -0.5 & 1.5 & -0.5 \\ -0.5 & -0.5 & 1.5 \end{bmatrix}$$

indicating that there is no asymmetry in the total effects of competitors on each other.

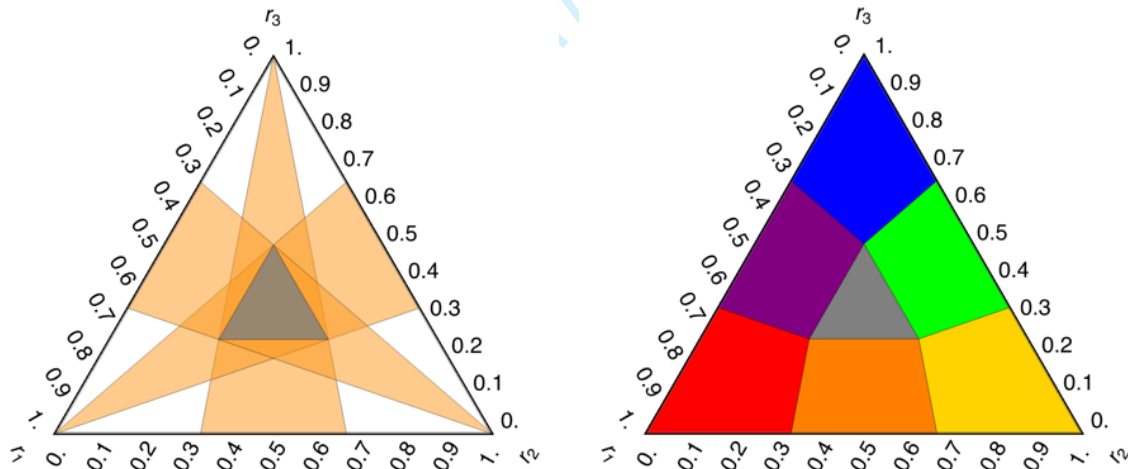


Figure F1. Feasibility and outcome plots with no cyclic asymmetry ($\bar{A} = 1$).

At a larger cyclic asymmetry value ($\bar{A} = 1.25992$), the three-species coexistence feasibility region completely overlaps the intersection of the three pairwise-feasibility regions (Fig. F2). In this case, the inverse competition matrix is

$$\alpha^{-1} = \begin{bmatrix} 1.333333 & 0 & -0.839947 \\ -0.839947 & 1.333333 & 0 \\ 0 & -0.839947 & 1.333333 \end{bmatrix}$$

The total effect of increasing r_1 on \hat{N}_3 is zero, which means that the direct negative effect of competition is perfectly balanced by the indirect effect mediated by their shared competitor species 2 (the enemy of my enemy is my friend).

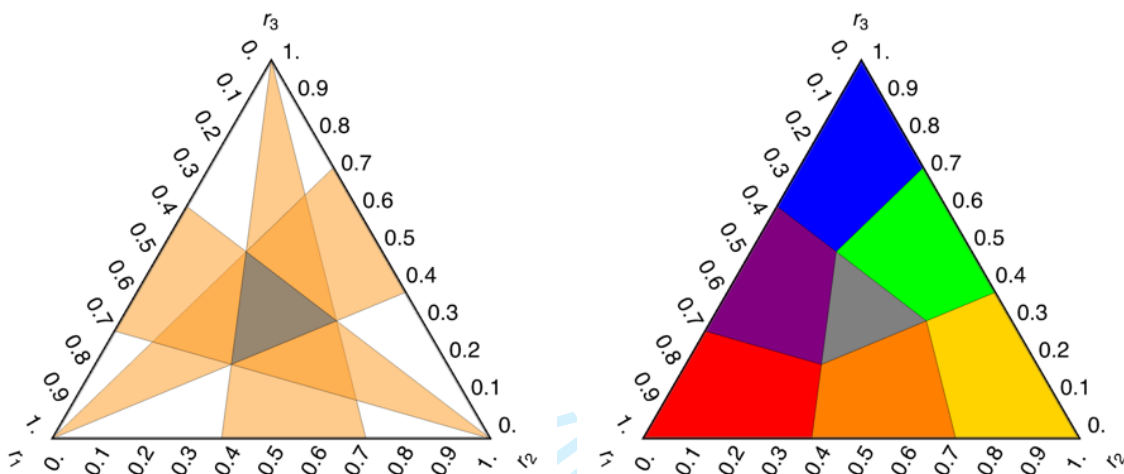


Figure F2. Feasibility and outcome plots with cyclic asymmetry $\bar{A} = 1.25992$.

At $\bar{A} = 2$, the three pairwise-feasibility regions intersect only in a point (Fig. F3). In this case, the inverse competition matrix is

$$\alpha^{-1} = \begin{bmatrix} 0.592593 & 0.592593 & -0.740741 \\ -0.740741 & 0.592593 & 0.592593 \\ 0.592593 & -0.740741 & 0.592593 \end{bmatrix}$$

Now the total effect of increasing r_1 on \hat{N}_3 is positive and equals its effect on \hat{N}_1 .

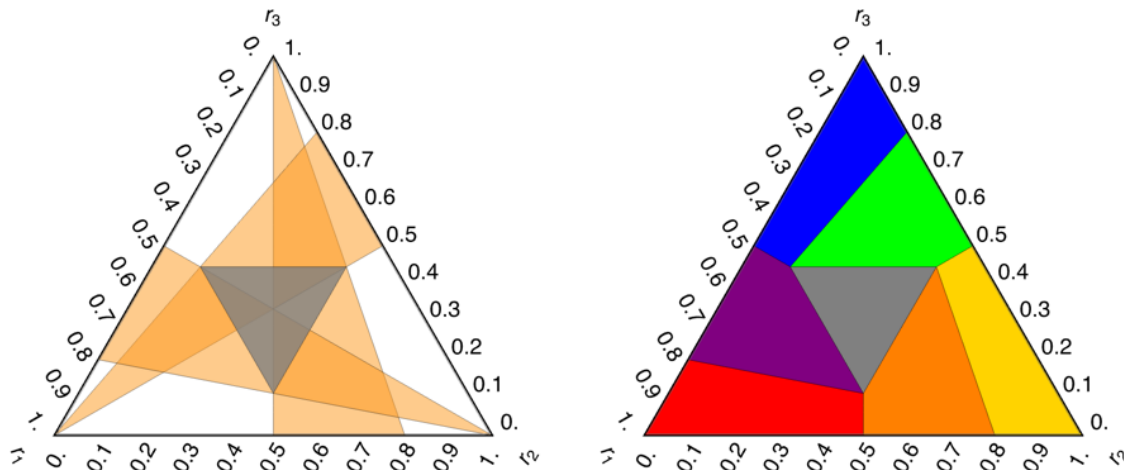


Figure F3. Feasibility and outcome plots with cyclic asymmetry $\bar{A} = 2$.

For larger cyclic asymmetry values ($\bar{A} > 2$), the three pairwise-feasibility regions cease to intersect, opening up a region of intransitivity at the center of the feasibility plot (Fig. F4). For example, when $\bar{A} = 3$, the inverse competition matrix is

$$\alpha^{-1} = \begin{bmatrix} 0.206633 & 0.57398 & -0.405612 \\ -0.405612 & 0.206633 & 0.57398 \\ 0.57398 & -0.405612 & 0.206633 \end{bmatrix}$$

The positive total effect of r_1 on \hat{N}_3 exceeds its effect on \hat{N}_1 , which results in the rock-paper-scissors dynamics.

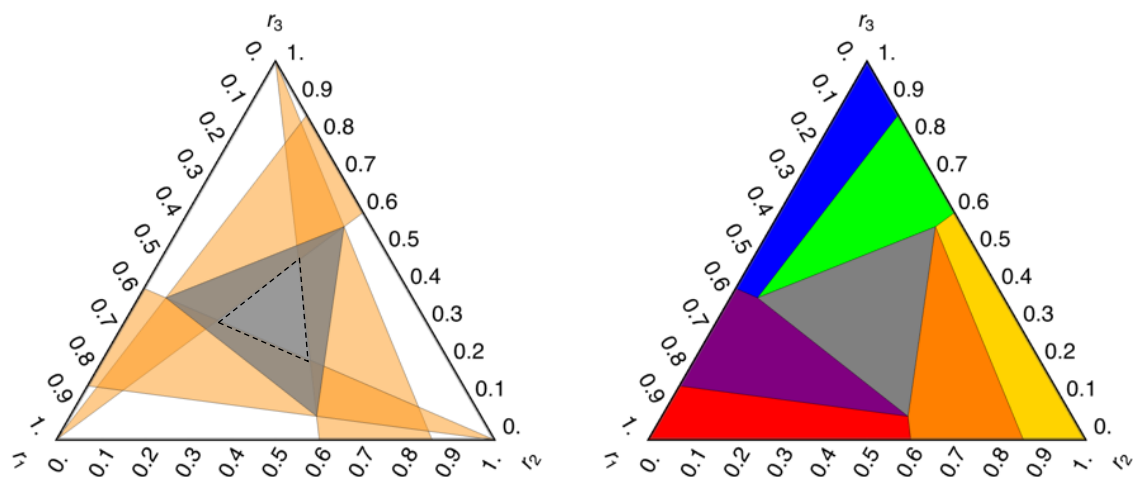


Figure F4. Feasibility and outcome plots with cyclic asymmetry $\bar{A} = 3$.

As shown in Fig. 3 in the main text, for larger values of cyclic asymmetry, a region of stable heteroclinic cycles emerges. However, nothing appears special about the structure of the inverse competition matrix at the bifurcation point $\bar{A} = 3.73205$:

$$\alpha^{-1} = \begin{bmatrix} 0.111111 & 0.496011 & -0.273789 \\ -0.273789 & 0.111111 & 0.496011 \\ 0.496011 & -0.273789 & 0.111111 \end{bmatrix}$$

Further investigation into the connection between the inverse competition matrix and the configuration of the feasibility and outcome plots may be fruitful.

References

- Bender, E. A., Case T. J., & Gilpin M. E. (1984) Perturbation experiments in community ecology: theory and practice. *Ecology*, 65, 1–13.
- Hofbauer, J. (1994). Heteroclinic cycles in ecological differential equations. *Tatra Mt. Math. Publ.*, 4, 105–116.
- Hofbauer, J. & Sigmund, K. (1988). The theory of evolution and dynamical systems : mathematical aspects of selection. Cambridge University Press.
- Hofbauer, J. & So, J.W.-H. (1994). Multiple limit cycles for three dimensional Lotka-Volterra equations. *Appl. Math. Lett.*, 7, 65–70.
- Klausmeier, C. A. (2008) Floquet theory: a useful tool for understanding nonequilibrium dynamics. *Theoretical Ecology*, 1, 153–161. <https://doi.org/10.1007/s12080-008-0016-2>
- Murata, Y. (1985). Modified Routh-Hurwitz (MRH) conditions for stability in cases of n=2, 3 and 4. *Oikonomika*, 22, 99–104.
- Saavedra, S., Rohr, R.P., Bascompte, J., Godoy, O., Kraft, N.J. & Levine, J.M. (2017). A structural approach for understanding multispecies coexistence. *Ecol. Monogr.*, 87, 470–486.
- Zeeman, M.L. (1993). Hopf bifurcations in competitive three-dimensional Lotka–Volterra systems. *Dyn. Stab. Syst.*, 8, 189–216.